THE UNIVERSITY OF MICHIGAN

INDUSTRY PROGRAM OF THE COLLEGE OF ENGINEERING

FLUID FLOW AT A SCRAPED HEAT TRANSFER SURFACE

Paul F. Youngdahl

January, 1961

IP-487

PREFACE

The problems encountered in designing a heat exchanger for very viscous fluids became evident during the work of the writer at Mechanical Handling Systems Inc. A unit was needed that would adjust fluid temperatures continuously, have low pressure drops, occupy a small space, and have modest power requirements. A scraped-surface heat exchanger at least partially fulfilled most of the demands, but no information was available in the literature to serve as a basis for design, although the principle dates back to the old-fashioned, hand-cranked ice cream freezer. This investigation was made to establish some of the factors which determine the mechanical design of a scraped-surface heat exchanger handling viscous fluids.

The writer wishes to express his appreciation to the members of his Doctoral Committee for their interest and advice, and to the mechanics in the Fluids' Laboratory for their help in constructing the experimental apparatus. Particular thanks are due to the Chairman of the Committee Professor Glen V. Edmonson and to Doctor Gordon J. Van Wylen for their encouragement and assistance.

The generous gift of "Ucon" fluid by the Carbide and Carbon Chemicals Company is gratefully acknowledged, and many thanks go to the Industry Program of the College of Engineering for their part in the final preparation of this dissertation. The assistance of Doctor F. H. Westervelt in the computer phases of this work is much appreciated.

Finally, the writer wants to express his gratitude to his wife and his family for their understanding during the years when this work was accomplished. The time it has required was taken from that which would have been spent with them.

TABLE OF CONTENTS

LIST OF TABLES

LIST OF FIGURES

LIST OF FIGURES (CONT'D)

NOMENCLATURE

B	number of scraper blades
C_p	specific heat - Btu/lb; °F
d	$R_o - R_i$ - Feet
F_d	apparatus dimensional factor - $\left(\frac{\ell}{1/R_i^2 - 1/R_o^2}\right)$
h	heat transfer film coefficient at scraped surface - Btu/hr; ft^2; °F
k	thermal conductivity - Btu/hr; ft^2; °F/ft
ℓ	axial length - feet
n	rotor speed - rps
n'	rotor speed - rpm
N_{Ta}	Taylor number, $\frac{d}{R_i}\sqrt{\frac{R_i \Omega_i d}{\nu}}$
$N_{Ta_{cr}}$	critical Taylor number for transition from laminar flow to vortex flow $\left[\frac{48.70(2 + \frac{d}{R_i})}{0.0571(1 - 0.652\frac{d}{R_i}) + \frac{0.00056}{(1 - 0.652\frac{d}{R_i})}}\right]^{1/2}$
R_i	radius of rotor - feet
R_o	radius of stator bore - feet
S	frequency of scraping surface - 1/hours
t	temperature - °F
Δt_{net}	temperature change of fluid due to heat transfer at the scraped surface - °F
Δt_{mech}	temperature rise of fluid due to mechanical effects - °F
T	torque - lbs (mass) ft^2/sec^2
T'	torque - inch pounds
V	speed of blade at scraped surface ft/hr
W	axial fluid flow rate lbs/hr

NOMENCLATURE (CONT'D)

μ	viscosity lb/hr; ft
μ'	viscosity - centipoises
ν	kinematic viscosity - ft^2/hr
ρ	density - lbs/ft^3
Ω_i	angular velocity of rotor - 1/hr

CHAPTER I

INTRODUCTION

This is an investigation of some of the factors which determine the mechanical design of scraped-surface heat exchangers handling viscous fluids. The fluid to be heated or cooled flows axially in an annular space between a stationary outer cylinder and a powered concentric rotor. The inner wall of the outer cylinder is the heat transfer surface which is scraped periodically by blades attached to the rotor. In this study, fluid viscosities are restricted to the 2,000 to 20,000 centipoise range, and the axial fluid flow rates are low.

Properly designed and applied, scraped-surface heat exchangers can be used economically in continuous processes to effect close control of the temperatures of products or reactants. Conventional batch heating or cooling of viscous materials, such as resins and prepolymers, in agitated vessels is slow, consumes much power, and requires large-size, expensive equipment. Although scraped-surface heat exchangers have been used in industry, the literature provides no basis for adequate mechanical or thermal design.

Objectives

The objectives of the laboratory observations, measurements, and analysis of this work using an experimental apparatus are as follows:

1. To determine the nature of the motion of the fluid in the passage between the rotor and the stator. Visual observations are made to reveal the action of the scraping blades on the fluid, and to show changes in this

action with variations in the type of blade, the number of blades, the viscosity of the fluid, and the speed of the rotor.

2. To determine the energy required to power the rotor. It is necessary to know the power demands in order to design the drive system. Much of the motive power is put into the fluid, and this energy imposes an additional load on the heat exchanger in cooling applications. Rotor torque requirements are measured as functions of speed, number of blades, and fluid viscosity.
3. To determine the order-of-magnitude heat transfer coefficients when the heat transfer surface is periodically scraped. Approximate heat transfer coefficients are determined to show the effects of the speed of rotation and the number of blades on heat transfer rates.

Description of Process

The experimental apparatus, described later, is typical of the components and arrangement of a commercial scraped-surface heat exchanger. The purpose of this section is to describe the nature of the fluid flow and heat transfer at an element of the scraped surface.

Within the fluid viscosity and flow rate limitations of this investigation, criteria indicate that both axial and rotational flows are primarily laminar. The prevailing mode of heat transfer between the surface and the fluid is conduction until the surface is scraped and the film is mixed with the bulk fluid. As long as flow is laminar, the axial velocity of the fluid does little to influence heat transfer coefficients.

A stepwise description of the process is as follows:

1. Bulk fluid is presented to the heat transfer surface. The full temperature gradient between the surface and the fluid is across the interface so that a relatively rapid transfer of energy occurs. The temperature distribution in a heating application is shown in Figure 1a.

2. The fluid next to the surface quickly approaches the surface temperature, and the temperature difference shifts to within the fluid. The energy transfer continues, but at a decreasing rate because the temperature difference occurs over a film of increasing thickness. The rate of heat transfer is limited by the thermal conductivity of the fluid which is generally low for viscous and resinous materials. The temperature distribution in a heating application is shown in Figure 1b.

3. When a scraper passes over the surface, it removes the thin film that has been heated or cooled. This film is mixed with the bulk fluid. The new temperature distribution is shown in Figure 1c.

4. New bulk fluid, which has some slight change in temperature due to the mixing of the heated or cooled film, is presented to the heat transfer surface, and the process repeats.

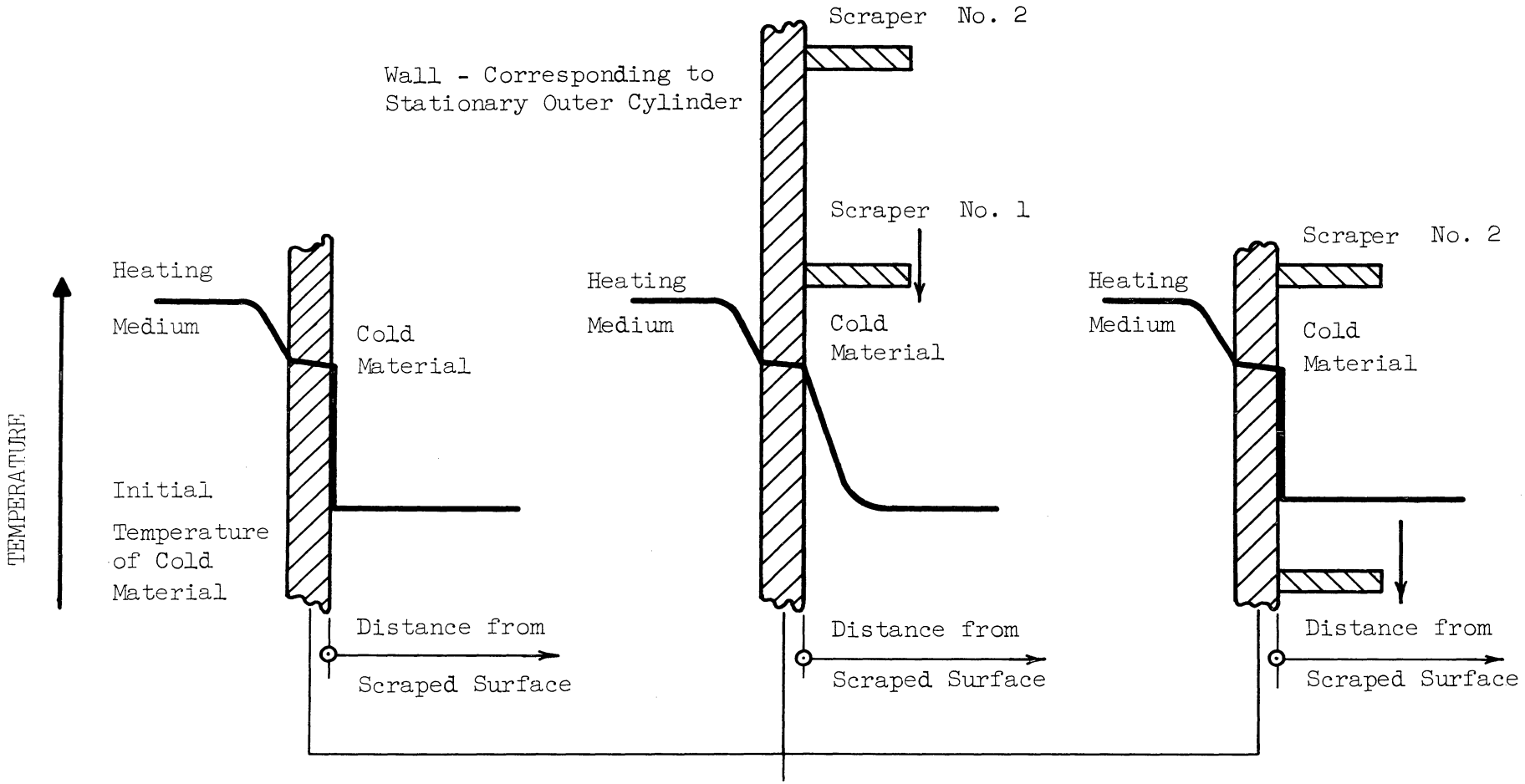

a) Initial contact of new cold material with surface

b) Just before first scraper passes surface

c) Just after first scraper passes surface

Figure 1. Schematic Representation of Temperature Distribution through One Scraping Cycle in a Heating Application.

Good scraper blades will completely remove the heated or cooled film from the surface, and will thoroughly mix it with the bulk fluid so that the maximum temperature differential can be maintained at the interface between the heat transfer surface and the fluid in contact with it.

Prior Work

The published literature reveals little concerning the design and performance of scraped-surface heat exchangers handling viscous fluids. The behavior of fluids between rotating concentric smooth cylinders has been the subject of considerable theoretical analysis and experimental work, and heat transfer rates in such systems have been explored under a variety of conditions. In the design analysis of this experimental apparatus, the fundamentals developed for smooth rotors are used to establish the mode of fluid flow for the no blade limiting condition.

The classical mathematical and experimental work of G. I. Taylor[15] provides a means for evaluating the stability of fluid flow in an annular space between concentric, rotating, smooth cylinders. Goldstein[4] expanded on Taylor's work to include the effects of axial flow of the fluid in the annular space. A mathematical approach was used to develop an equation for calculating the angular velocity for which flow just becomes unstable for a given axial Reynolds member. He shows that under laminar flow conditions the axial and rotational flow characteristics are independent of each other, and that the torque required for a given rotational speed is independent of the axial-flow

velocity. The torque requirements of a smooth rotor system can be calculated from the Reiner and Riwlin equation for the rotational viscometer as in Green's[5] discussion of the forces and stresses in various classes of fluids.

Gazley[3] investigated heat transfer with rotational and axial flow between concentric cylinders as in the gap between the rotor and the stator in rotating electrical machinery. He used a Reynolds number based on the peripheral speed of the rotor to establish modes of flow, and concludes that steady-state heat transfer across an annular gap for laminar flow is accomplished by pure conduction.

Kaye and Elgar[8] investigated modes of flow for adiabatic and diabatic flow of air in annuli with an inner rotating smooth cylinder and an outer stationary cylinder. They established a new dimensionless group called the Taylor number which is used with an axial Reynolds number to establish four modes of fluid flow, i.e., laminar flow, turbulent flow, laminar flow plus vortices, and turbulent flow plus vortices. The heat transfer aspects of their work shows the Nusselt number remains constant in the laminar-flow regime.

Bjorkland and Kays[1] used air in the annulus of a system of concentric rotating cylinders to show that heat transfer rates indicate three regimes of flow, i.e., (a) laminar flow with heat transfer by conduction, (b) vortex flow which increases the heat transfer rate, and (c) distorted vortex flow. Equations are presented to calculate a ratio of actual Nusselt number to a conduction Nusselt number in terms of the Taylor number and dimensions of the apparatus. Jacob and Rees[7] developed equations for heat transfer coefficients for systems of smooth rotating cylinders where both axial and rotational flows are laminar.

In a water-to-water scraped-surface heat exchanger, Houlton[6] evaluated overall heat transfer coefficients experimentally. Rotor speeds and axial fluid flow rates were both high so that the mode of flow without blades would have been other than laminar. He developed no equations for calculating film coefficients at the scraped surface, and he did not determine the power requirements. Kool[10] made a mathematical analysis of the heat transfer coefficient of a scraped-surface heat exchanger handling viscous fluids. The theoretical equation which he developed assumes that all of the fluid is scraped from the surface with each pass of a blade, and that the heated or cooled scraped film is mixed completely with the bulk fluid. He illustrates how a residual thin film on the scraped surface will decrease the heat transfer coefficient, and he notes that incomplete mixing after scraping, as is obtained in practice, will cause a further lowering of an actual coefficient.

In one of his earlier papers, Skelland[11] used dimensional analysis to develop an equation from experimental data for calculating heat transfer rates in a scraped-surface heat exchanger. Later papers recommend changes to this equation because of probable errors. Kern[9] indicates that Skelland's equation, even if correct, would be misapplied in the case of pure laminar flow, and that the viscous core of fluid between the scrapers and the rotor body in is laminar flow rotationally as well as axially.

Skelland, Oliver, and Tooke[14] arranged the variables affecting heat transfer rates in a scraped-surface heat exchanger into dimensionless groups, and by experiment, they evaluated the constants and

exponents to give equations for calculating film coefficients. Two equations were presented, one for the case of cooling viscous liquids, and one for the case of cooling thin, mobile liquids. There are considerable discrepancies between the results of this work and that of Skelland,[12] and explanations are given to show why the later work is more nearly correct.

In the only published work regarding power requirements of scraped-surface heat exchangers, Skelland and Leung[13] arranged the significant variables into dimensionless groups, and by experiment, established a coefficient and exponents for a Reynolds number and for the number of scraping blades group. Two different equations for making the same calculation are presented, and the necessity of doing additional work to establish accurate values is emphasized.

The above references are cited here to indicate their scope and content, but detailed comments and comparisons are made in later sections where the application is direct.

CHAPTER II

DESCRIPTION OF APPARATUS AND EXPERIMENTAL PROCEDURE

The basic unit in the experimental apparatus is the rotor-stator assembly. It consists of a driven rotor within a stationary concentric tube. The rotor is solid aluminum with fittings for attaching 0 to 4 axial blades which scrape the inside surface of the outer cylinder. This stationary outer cylinder is a precision-bored glass tube for making the visual studies and torque measurements. A composite tube made of a water-jacketed steel section between two glass ends is used for making the heat transfer observations.

A four-speed, rotary, floating drive is arranged to measure torque demands through a strain gage transducer. The rotor speed is measured on the input side of a 10 to 1 fixed ratio gear reducer. The working fluids are water solutions of "Ucon"* 75-H-90,000 covering the full viscosity range of 2,000 to 20,000 centipoises. The circulating systems for the primary fluid and the heat transfer fluid complete the equipment.

Rotor-Stator Assembly

The arrangement and principal dimensions of the rotor-stator assembly with the glass tube are shown in Figure 2. The viscous fluid is admitted at the bottom of the apparatus, through four 3/4 inch standard pipe connections, into a distribution plenum, and flows axially, through the annulus, to the top. The collecting pan directs the fluid,

---

* Trademark, Carbide and Carbon Chemicals Company

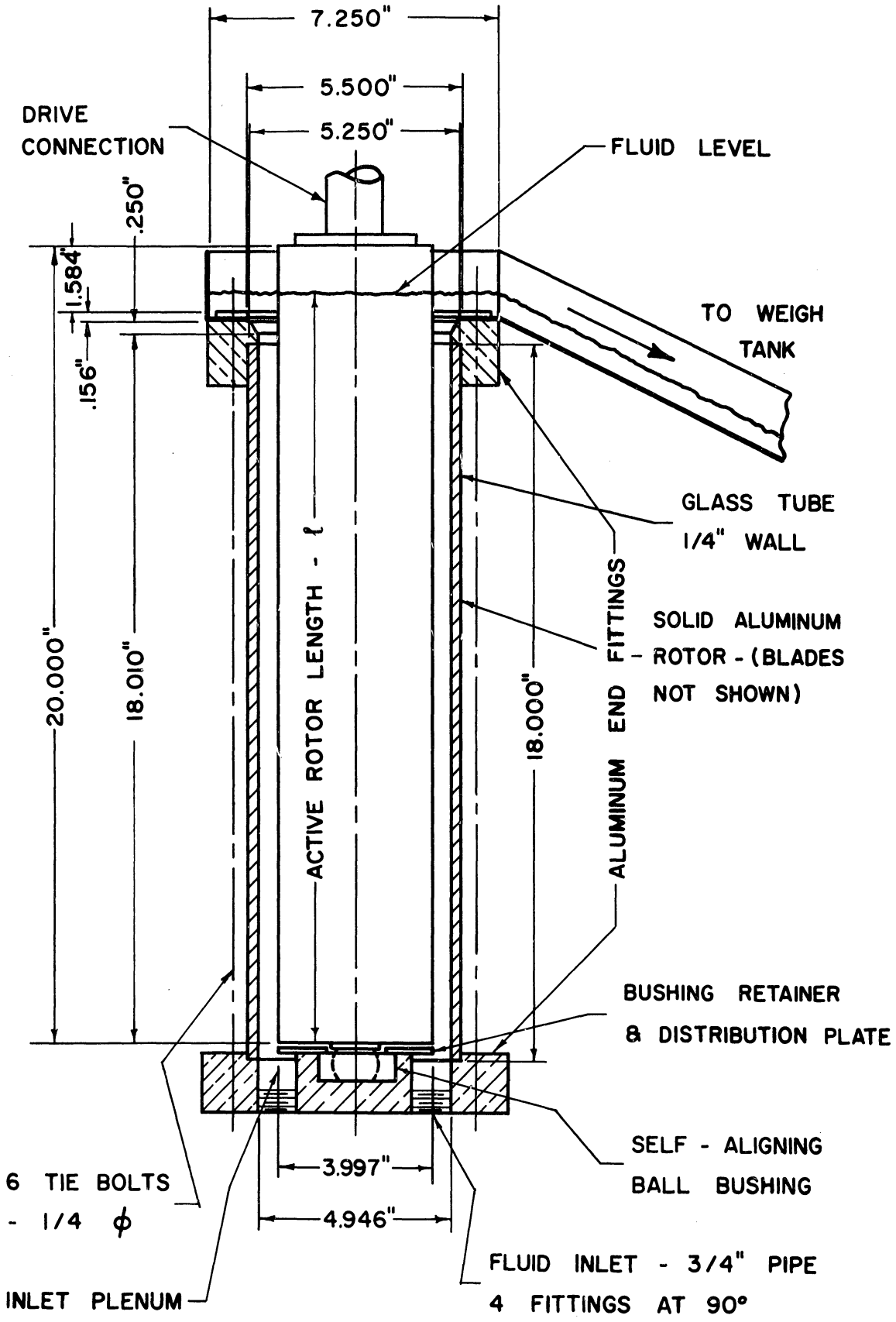

Figure 2. Rotor-Stator Assembly with Glass Tube.

as it overflows, to the open channel which drains into the weigh tank. The bore of the glass tube and the diameter of the rotor are within $\pm$ 0.002 inches of the nominal dimensions shown on the drawing, including out-of-round tolerances. In the assembly of the rotor and stator, concentricity is held to within a tolerance of 0.003 inches. All axial dimensions are correct to $\pm$ 0.005 inches.

The level of the fluid in the system must be considered when the experimental data are calculated. This level changes as a function of flow rate, viscosity, and rotor speed, and the effective diameter of the outer member changes with the level. The Reiner and Riwlin equation for smooth rotors can be applied because the blades do not extend into the area of changing fluid level and stator diameter. With a rotating inner member and stationary outer member, this equation is

$$T = 4\mu\pi\ell \frac{\Omega_i}{\frac{1}{R_i^2} - \frac{1}{R_o^2}} \quad . \tag{1}$$

For convenience in making later calculations, it can be simplified by substituting constants and grouping terms. All terms relating to the dimensions of the apparatus are included in the expression

$$F_d = \text{dimensional factor} = \frac{\ell}{\frac{1}{R_i^2} - \frac{1}{R_o^2}} \tag{2}$$

which varies with the length of the rotor which is exposed to the fluid. This dimensional factor is plotted against the active rotor length in Figure 3. Introducing conversion factors and substituting (2), Equation (1) becomes

$$T' = 1.909 \times 10^{-7} \ \mu' n' F_d \tag{3}$$

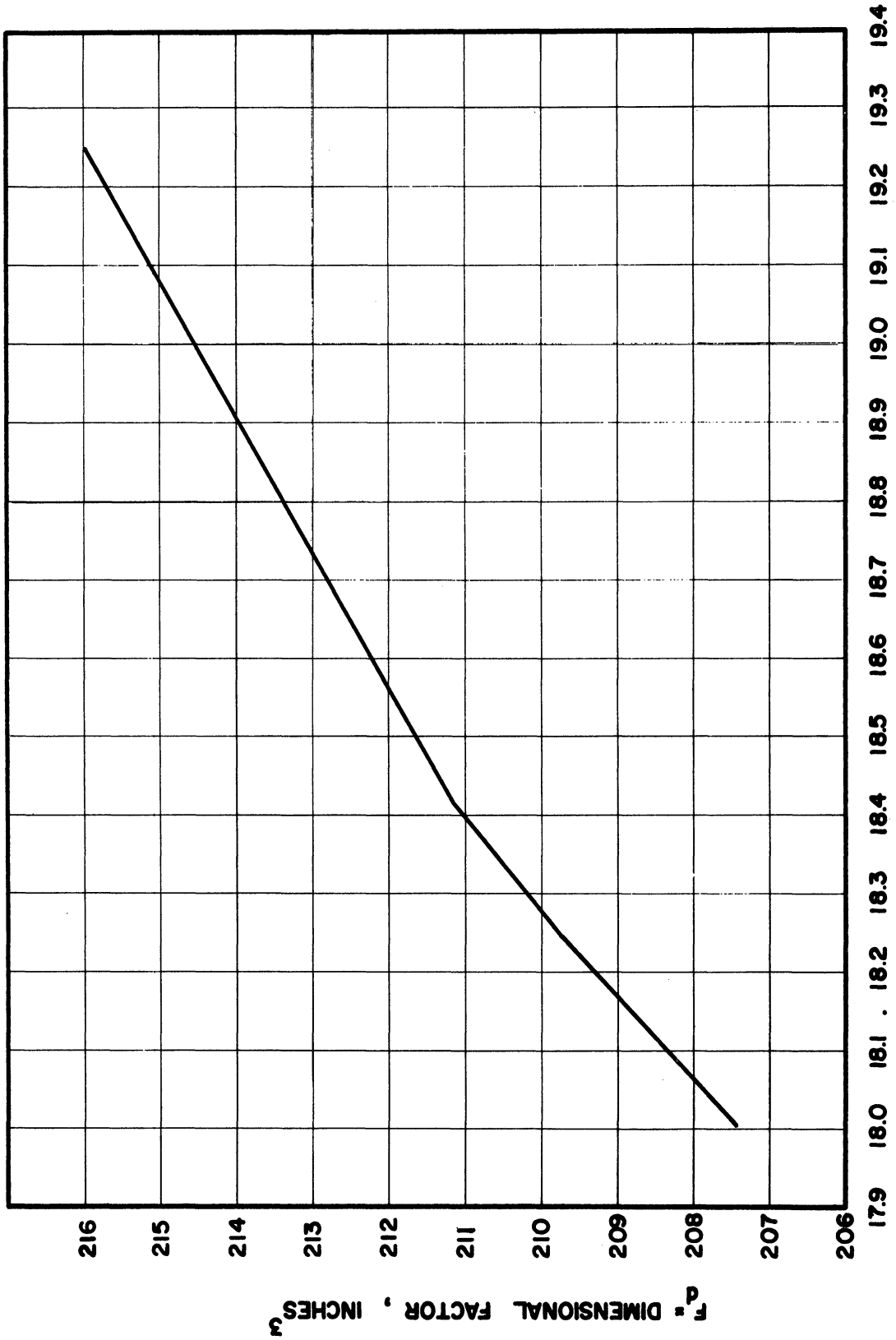

Figure 3. Dimensional Factor versus Active Rotor Length.

where

T' = rotor driving torque in inch pounds (force)

μ' = fluid viscosity in centipoises

n' = rotor speed in rpm

F_d = dimensional factor in inches^3.

The Reiner and Riwlin equation, and thus Equation (3), assumes the rotational flow of the fluid to be laminar. Taylor[15] established the criteria for determining when instability in rotational flow just starts. Using the notation of Bjorklund and Kays,[1] a dimensionless Taylor number is defined,

$$N_{Ta} = \sqrt{\frac{d}{R_i}} \frac{R_i \Omega_i d}{\nu} \tag{4}$$

and the critical Taylor number is

$$N_{Ta_{Cr}} = \left[\frac{48.70(2 + \frac{d}{R_i})}{0.0571(1-0.652 \frac{d}{R_i}) + \frac{0.00056}{(1-0.652 \frac{d}{R_i})}} \right]^{1/2} . \tag{5}$$

When the Taylor number is less than the critical Taylor number, rotational flow is laminar. Goldstein[4] and Kaye and Elgar[8] show that the additional of an axial component either does not affect rotational flow or may make it slightly more stable.

For a dimensionally similar smooth rotor apparatus, the critical Taylor number is 47.2. Assuming the minimum fluid viscosity of 2,000 centipoises and the maximum rotor speed of 170 rpm, the Taylor number is 2.77. Although the addition of blades to the rotor may change the magnitude of the Taylor number slightly, rotational flow can be clearly classified as laminar.

Heat Transfer Stator

For heat transfer measurements, the stationary cylinder is modified to include a water-jacketed steel surface which is scraped by the rotor blades. Figure 4 shows the arrangement and dimensions of the heat transfer tube. The total scraped area is 0.858 ft^2. Thermocouple numbers 5 and 6 are inserted into small drilled holes at each end of the steel heat-transfer tube. The bead is brought to the surface and then peened flush with the surface. The thermocouple leads are secured by potting with epoxy resin.

Other thermocouples are used to measure temperatures as follows:

Thermocouple No.	Location and Temperature Measured
1	Primary fluid inlet temperature in inlet plenum.
2	Same as No. 1 except on opposite side of plenum.
3 & 4	Primary fluid outlet temperature in fluid film near bottom of open channel to weigh tank.
5 & 6	Heat transfer surface temperature as noted in Figure 4.
7	Heating or cooling water inlet temperature in inlet plenum.
8	Heating or cooling water outlet temperature in outlet plenum.

All thermocouples were calibrated at the ice point, steam point, and decomposition temperature of sodium sulphate decahydrate (90.27°F).

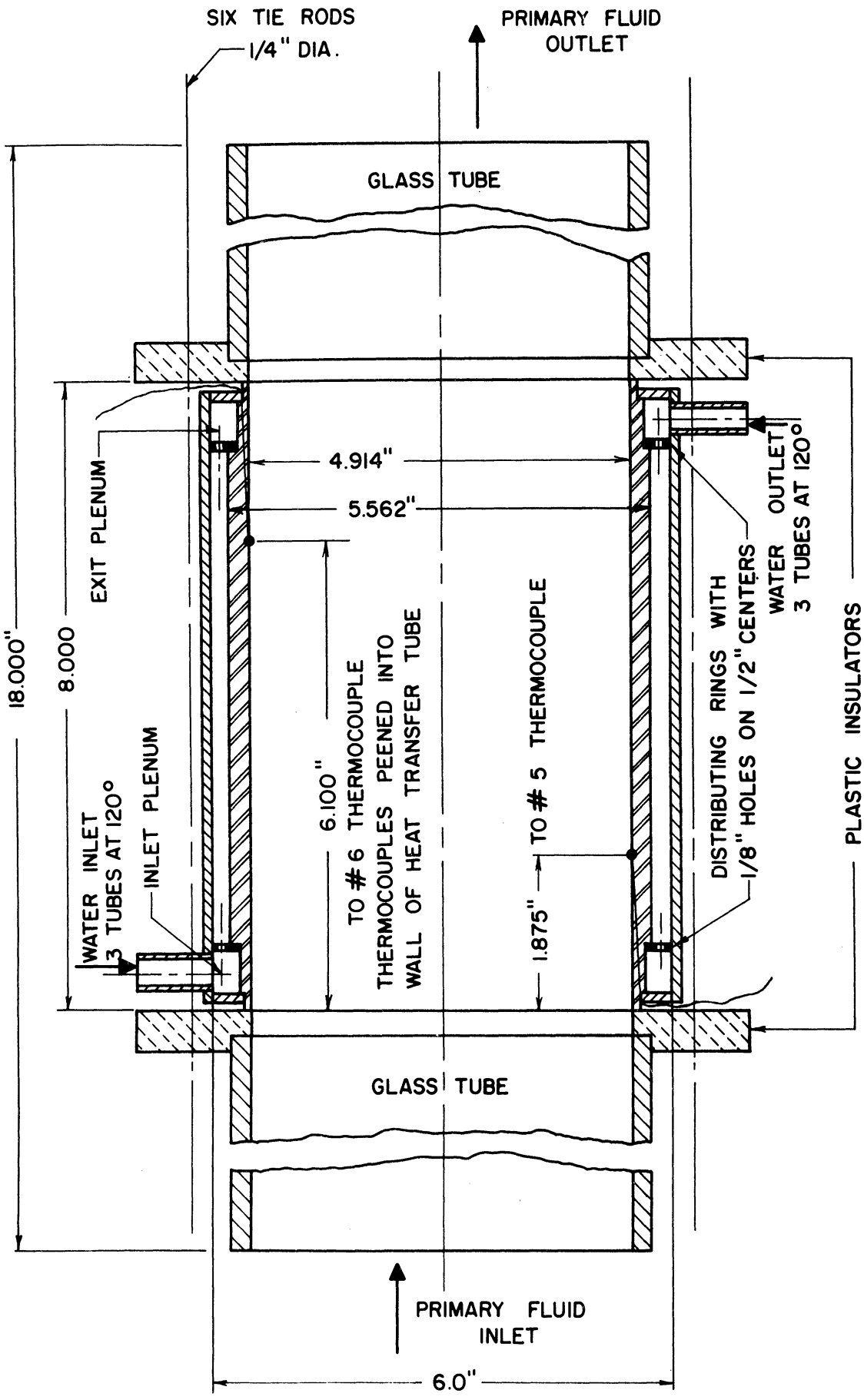

Figure 4. Heat Transfer Tube.

Rotor and Blades

The rotor body is solid aluminum, 20 inches long and 3.997 inches in diameter. Drilled, tapped, and counterbored holes for holding blade attachments are located as shown in Figure 5. The brass end-fittings were fitted before the final turning of the rotor outside diameter to insure concentricity. When one or more blades are not used, the attaching holes are plugged with "Allen-Head" screws and putty to make a smooth surface.

The two types of blades and the detail of the blade attachment are shown in Figure 6. The springs in the blade attaching fittings were selected to have the minimum force to just cause the blades to contact the surface without adding mechanical drag to the system. The type A blade spans the entire annular space between the rotor and stator. Type B blade is designed to scrape the entire heat transfer surface, but maximum clearance is maintained for fluid flow between the scraping blade and the rotor body.

Drive-Speed and Torque Measuring

The rotor is driven by an electric motor through a V-belt and pair of 4-step pulleys to a countershaft. A V-belt and pulleys connect the countershaft to the input of a worm-type gear reducer which connects directly to the rotor power fitting. The general arrangement is shown in Figure 7.

The significant design feature of the drive is the mounting arrangement so that all elements in the power train are free to turn, as an assembly, about the main power shaft centerline. A plate bolted to

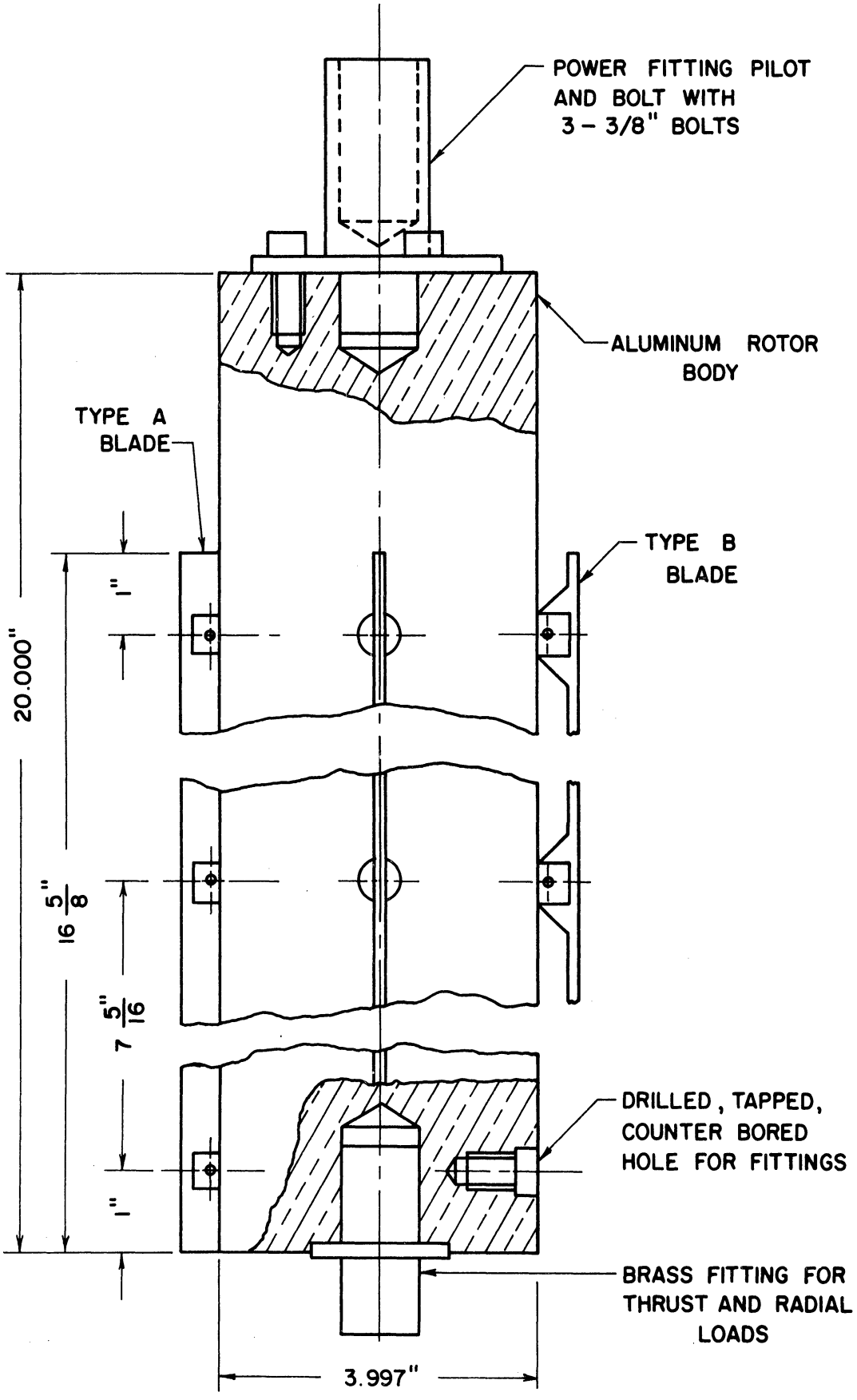

Figure 5. Rotor and Blade Assembly.

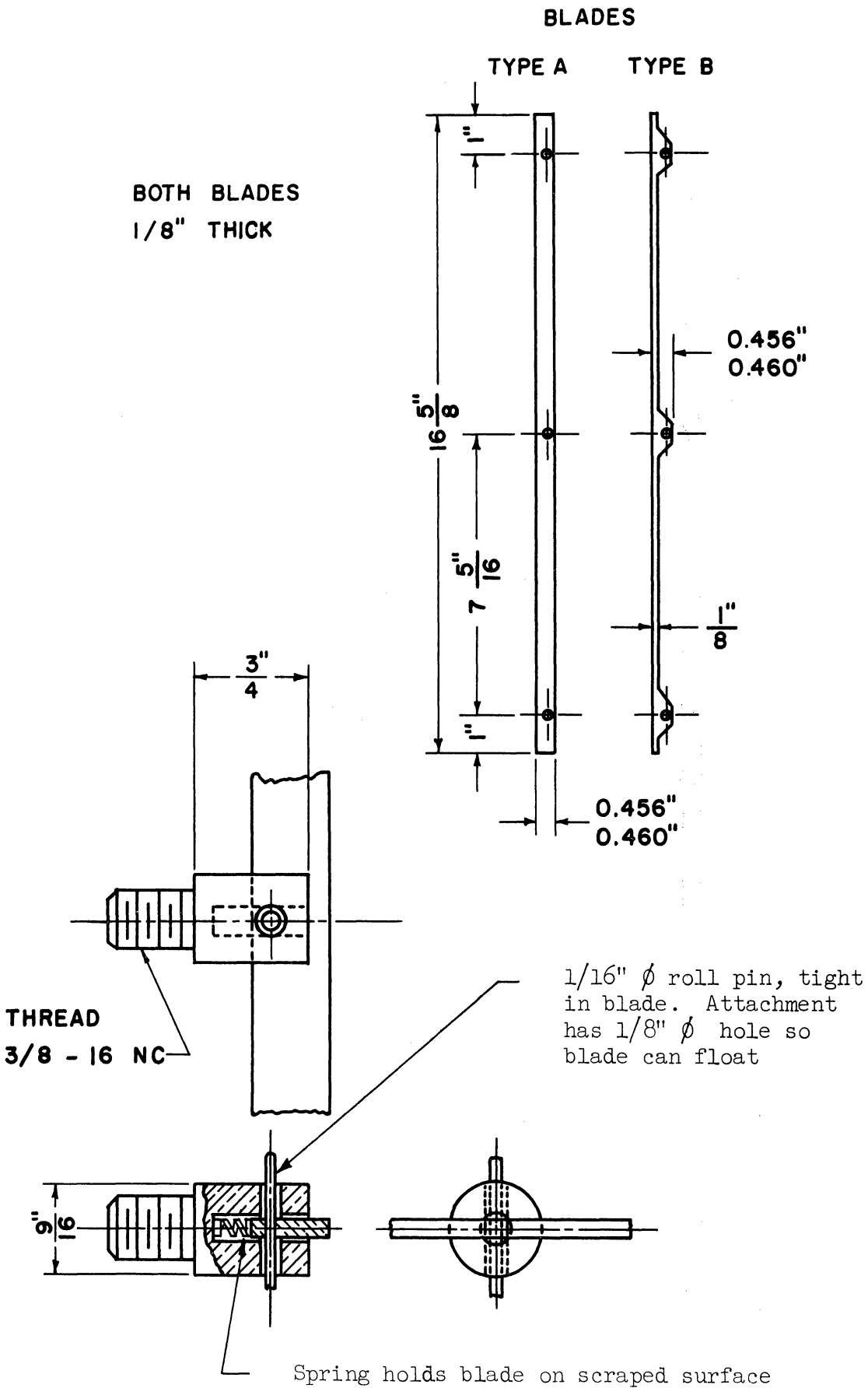

Figure 6. Scraping Blades and Attachments.

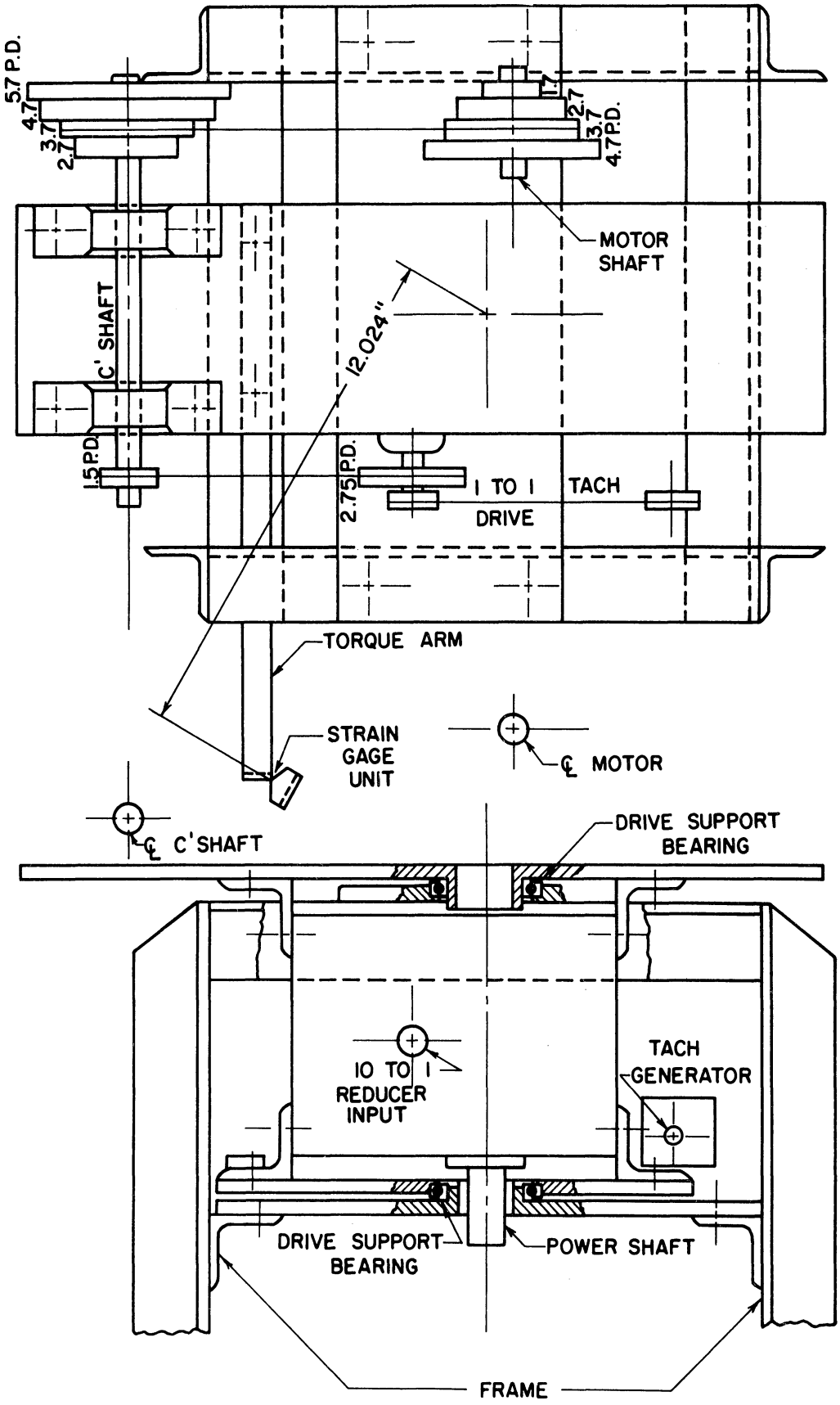

Figure 7. Drive Arrangement.

the top of the worm-gear reducer holds the motor and countershaft, and is machined to receive the inner race of the top drive-support bearing. A second plate is bolted to the bottom of the reducer, and is machined to receive the outer race of the lower drive-support bearing. The other race of each bearing is fitted to respective upper and lower plates, bolted to the rigid, main-support frame. The bearings are an aircraft type and quality with no seals or retainers. The radial and axial capacities are well over the load imposed.

The tachometer generator is driven from the reducer input shaft through a cogged "timing" belt and pulley arrangement. The timing belt drive is a 1-to-1 ratio, so indicated speed is exactly 10 times true rotor speed because of the 10-to-1 ratio of the reducer. The tachometer generator is bolted to the reducer, so it too becomes a part of the rotating assembly.

The drive machinery, mounted on the bearings, is restrained from rotating by a torque arm attached to the reducer. The force developed at the end of the arm is measured with a combination of a strain-gage instrumented cantilever beam and a pan-balance and weights. The effective length of the torque arm is 12.024" ($\pm$ 0.002"). The torque arm has a point-bearing on the strain beam, and at the knife-edge, cords are attached which lead over bearings to support weight pans. Two pans are used so the weights on each are opposing. The one acts in the direction to impose a load on the strain beam, and is used for calibration. The balance pan and weights act in the opposite direction so that their effect is additive to the strain indicator reading. The total force exerted by the torque arm is the sum of the weights on the balance pan and the force on the strain transducer.

The instrumented strain transducer is shown in Figure 8. Once mounted and clamped in place, it was calibrated, and then was not moved or loosened. The calibration curve shown as Figure 9, was obtained by placing dead weights, in 1/8 pound increments, on the calibration pan described above. The calibration was accomplished with the motor and all floating drive machinery running, but the coupling to the rotor disconnected. The gage factor adjustment on the SR-4 indicator was used to reset the zero point to a dial reading of 480 before each run. Frequent checks throughout the experimental work showed that linearity and calibration was maintained. The accuracy of the system is such that it can be read to $\pm$ 0.01 pounds. The greatest probable error because of needle swing, damping, friction, etc., is $\pm$ 0.05 pounds.

Primary Fluid Circulating System

The primary fluid circulating system, shown in Figure 10, is designed to provide intermittent flow through the test apparatus. A 30 gallon pressure tank is filled with the fluid of the viscosity desired for a particular run and blanketed with air at a controlled pressure. The fluid is forced through a delivery line, into a pipe manifold, through four hoses, to the bottom plenum of the rotor and stator assembly. It flows upward in the annular space between the rotor and the stator, and as it overflows the stator tube, it is collected in an attached pan with one side open. The open side of the pan connects to a sheet metal channel that permits the fluid to flow by gravity into the weigh tank on a platform scale. The discharge of the weigh tank is kept

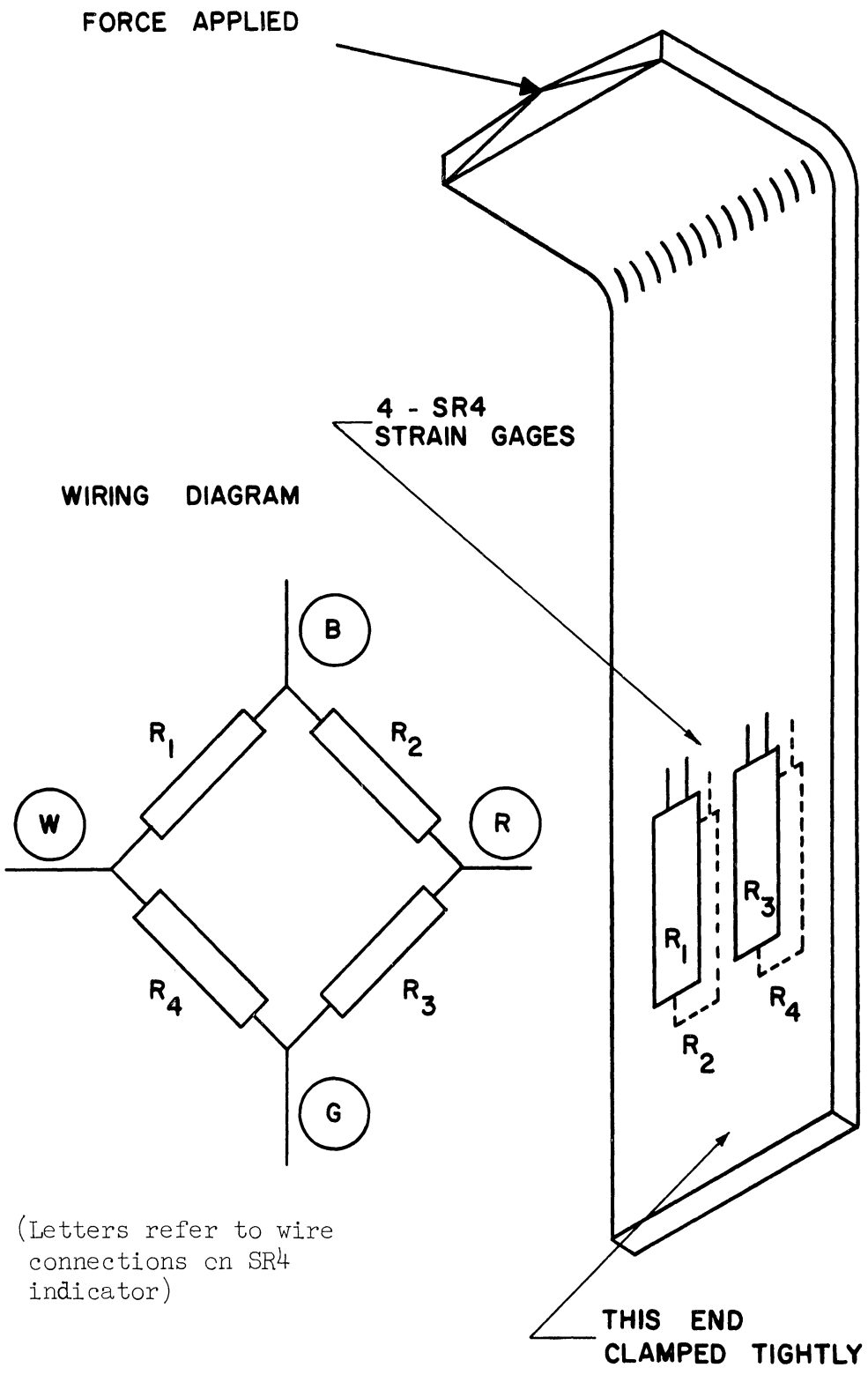

Figure 8. Strain Transducer for Torque Measurement.

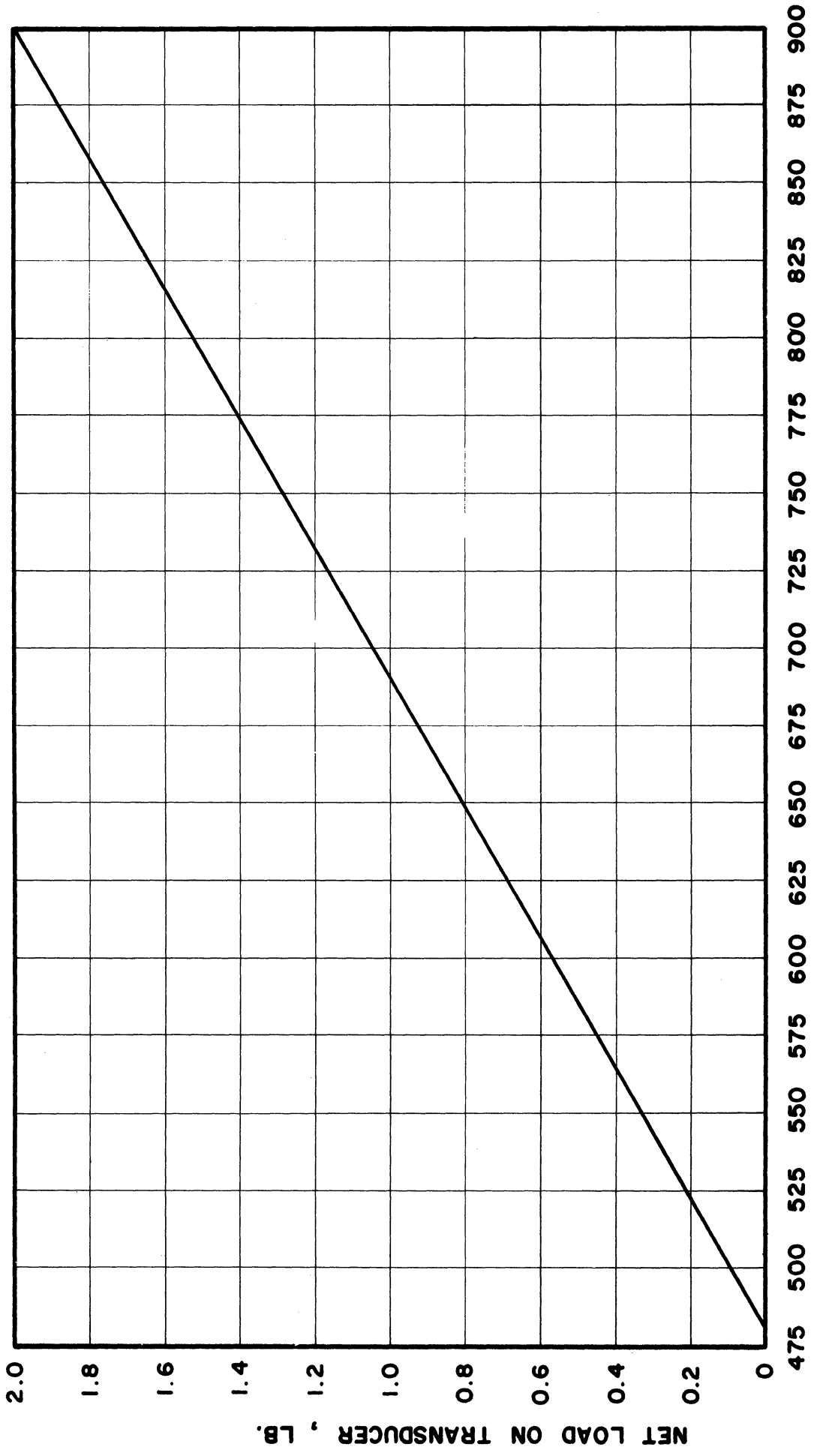

Figure 9. Strain Gage Dynamometer Calibration.

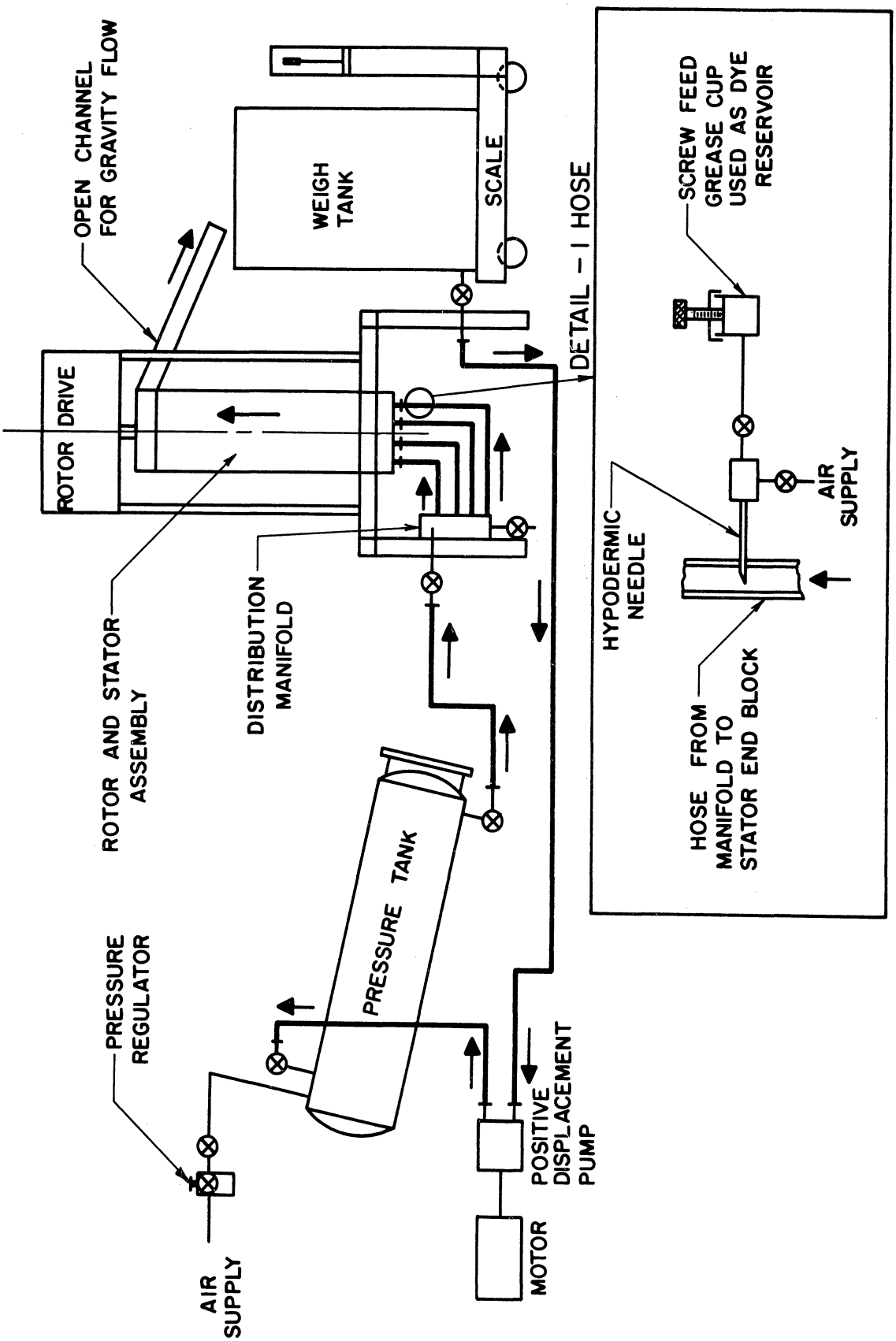

Figure 10. Primary Fluid Circulating System.

closed until the end of the run, and the scale is periodically balanced to indicate flow rates. At the end of a run, the fluid collected in the weigh tank is pumped back into the pressure tank, and the cycle repeats.

The inset in Figure 10 shows the method used to introduce air bubbles or a dye into the main fluid for making some of the visual studies. Food coloring is mixed with a small amount of the test fluid of the viscosity being used, and is placed in a pressure-feed grease cup. The discharge of the grease cup is connected to a hypodermic needle which is inserted into one of the hoses attached to the rotor-stator assembly. A turn of the screw feed will introduce one or more drops of a colored fluid with approximately the same viscosity as the primary fluid. An air connection to the same hypodermic needle permits air bubbles to be introduced in a similar manner.

Heat-Transfer Fluid Circulating System

A schematic diagram of the system for circulating hot and cold water in the jacket of the heat transfer tube is shown in Figure 11. A supply manifold and a return manifold each have three connections for rubber hoses which attach to corresponding fittings on the heat transfer tube. The water flows in the bottom and out the top of the annular jacket surrounding the steel cylinder that has its inside surface scraped by the blades.

In heating runs, the water is circulated with a positive displacement pump at a rate of about 4 gpm. The 1000 watt heater has a self-contained thermostat that controls the temperature on an on-off basis. A reservoir, fabricated from large-size pipe, holds the heater and feeds

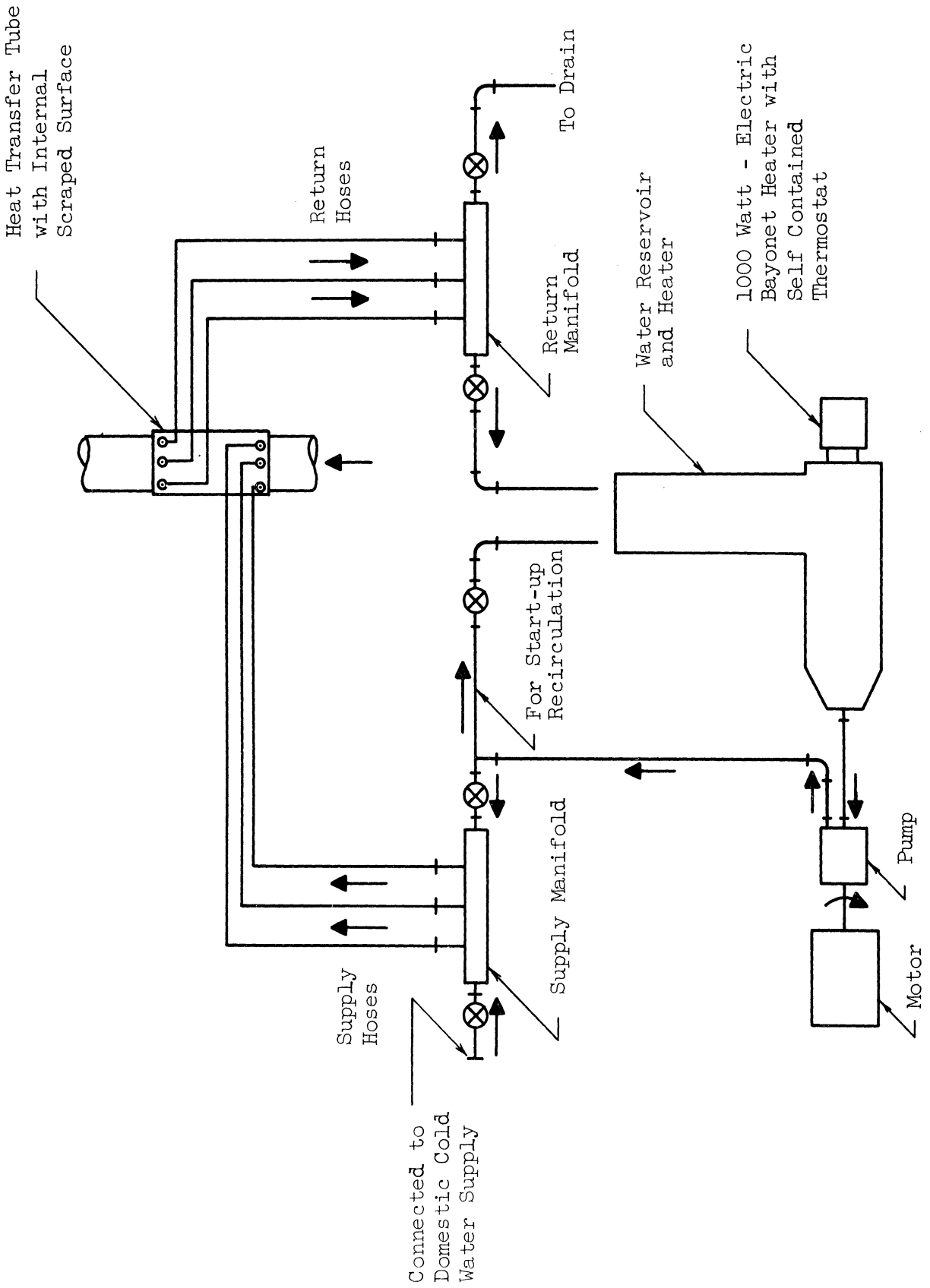

Figure 11. Heat-Transfer Fluid Circulating System.

the inlet of the pump. The water leaving the jacket returns to the reservoir, through the return manifold, by gravity. A by-pass recirculation line is provided for start-up.

In cooling runs, the hot water connections are shut off from the manifolds, and domestic cold water feeds the supply manifold. The spent cooling water is directed to drain when it leaves the return manifold.

The Primary Fluid

After an investigation of several water-mixed and water-soluble materials, Ucon 75-H-90,000 was selected as the working fluid. The characteristics which are desired and which determined the choice are:

a. the complete viscosity range of 2,000 to 20,000 centipoises can be obtained by mixing different amounts of water with the base fluid,

b. the fluid and its water solutions are stable and they will maintain the same viscosity over the entire test period,

c. the rheological classification of the fluid and its solutions is Newtonian,

d. the fluid presents no health hazard in its use.

Other materials which were investigated for use include water solutions of cellulose gums and a high molecular weight polymer of ethylene oxide. The viscosity of the latter (Polyox* WSR301) shows a marked

---

* Trademark - Union Carbide Chemicals Company

dependence on shear rate, and was rejected for this reason. The ropy consistency or stringiness of the water solutions of the Polyox resin would probably be objectionable.

Water solutions of sodium carboxymethylcellulose (CMC) were considered because of the small percentages of CMC required to attain the desired viscosities. Although the measured viscosities of the solutions were somewhat responsive to shear rates, the effect was not marked. Beaker samples of the proposed solutions appeared quite stable, but full scale quantities showed a considerable loss of viscosity during storage. The change in viscosity was attributed to biochemical action even though a preservative (sodium benzoate) was added.

The properties of Ucon 75-H-90,000 and its water solutions were determined by measurement and from information supplied by the manufacturer's catalog (Union Carbide Chemicals Company). It is classified as an unrefined polyalkylene glycol-type fluid containing 0.07% of an alkaline material calculated as potassium hydroxide. A blackening and slight etching of the aluminum rotor is the only noted effect of the fluid on the equipment.

A Brookfield Model LVF Synchro-Lectric Viscometer with four spindles and four speeds is used to measure viscosities. During each run, a viscosity determination was made at several different shear-rates at the temperature of use. From these accumulated data, temperature-viscosity curves were drawn and the viscosity of various concentrations is determined at 75°F. A plot of the viscosity of water solutions of Ucon 75-H-90,000 is shown in Figure 12. This curve is presented for

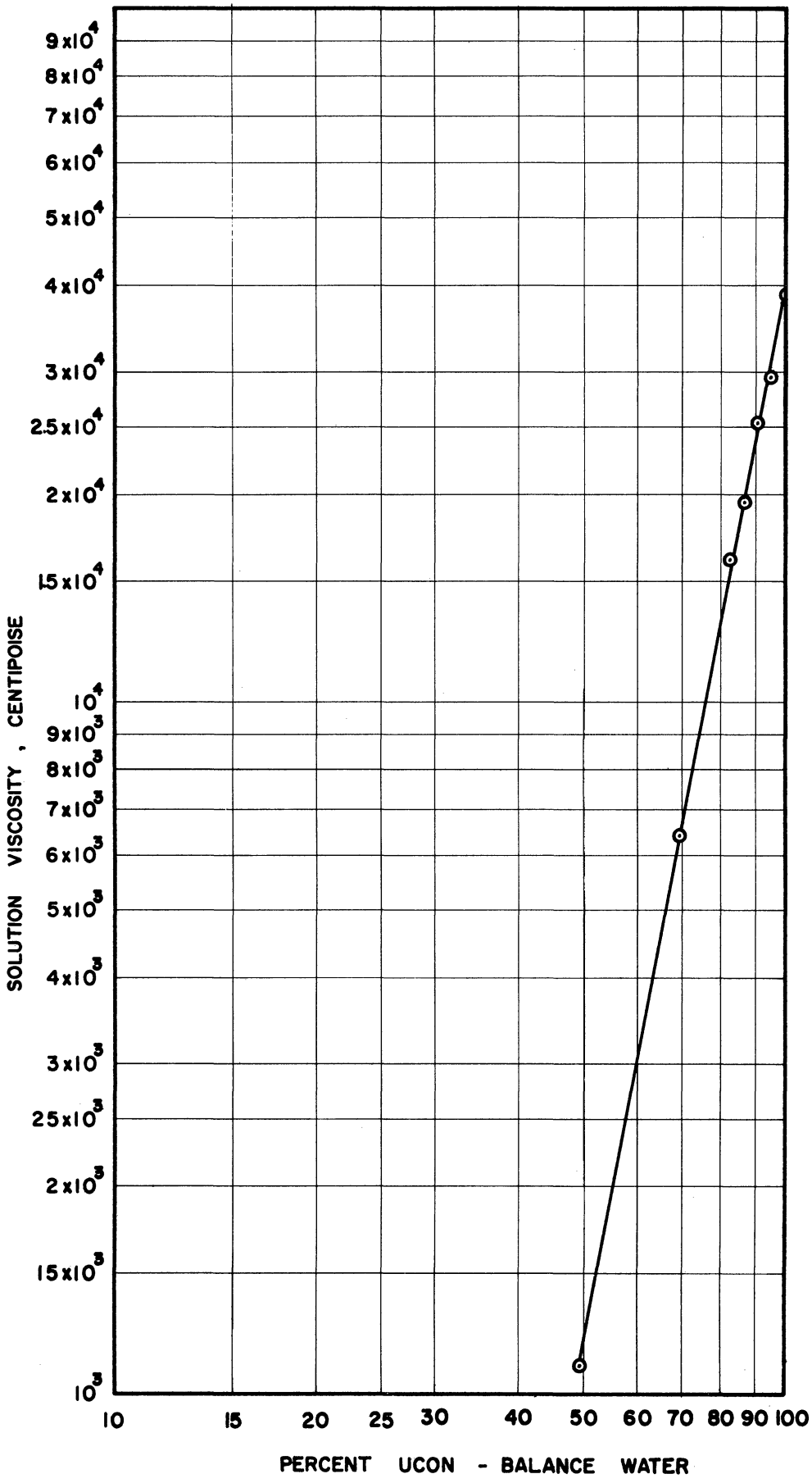

Figure 12. Viscosity of Ucon-Water Solutions at 75°F.

for reference only, because the actual observed viscosities for each run are used in all calculations.

Other fluid properties of interest in the heat transfer phases are specific heat and thermal conductivity. Using the data of Curme and Johnston[2] for aqueous solutions of glycols, the equations from the International Critical Tables, and the manufacturer's data the following values are obtained:

Solution Viscosity at 75°F - Centipoises	Percent Ucon	Thermal Conductivity Btu/hr; ft^2; °F/ft	Specific Heat Btu/lb; °F
10,700	77.5	0.131	0.62
15,100	83.0	0.121	0.59

Experimental Procedure and Technique

The experimental work can be divided into three phases as follows:

1. visual observations,
2. torque measurements,
3. heat transfer determinations.

During any one of these phases, the following factors can be varied:

1. rotor speed - Four belt positions on the step-cone pulleys give approximate rotor speeds of 32, 60, 95, and 150 rpm. The actual rotor speed is influenced by belt slip and motor response under load. The rotor speed is measured several times during each run.
2. fluid viscosity - Four basic solutions have been prepared to cover the full viscosity range with nominal

values of 2,000, 8,000, 14,000, and 20,000 centipoises. The actual solution viscosity is influenced by its temperature (ambient) at the time of the run. The exact fluid viscosity is measured several times during each run.

3. scraper blades - The scraper blades constitute a variable in the following two ways:
   a. number of blades - The rotor is operated with 0, 1, 2, or 4 blades.
   b. blade design - Both type A and type B blades, described above, are radial and spring-loaded. The design difference is basic in the blade action on the core material next to the rotor.

Torque measurements were made with all combinations of all of the above variables, but the full scope of variables was not explored in the heat transfer phases. It was convenient to observe the significant changes in the action of the rotor and blades on the fluid during the torque measurement set-up.

Before any observations or readings were taken, the system was operated long enough to attain steady-state conditions. For the visual parts, the prepared dye of the same viscosity as the fluid was forced into the inlet stream. The motion of the dye streak could be readily followed at the lower rotor speeds, and the general flow pattern could be established even at the top speed. The pressure gradient from the leading face of one blade to the following face of another blade was determined by operating the tube partially filled with fluid and measuring the difference in fluid height.

For each given rotor speed, type of blade, number of blades, and fluid viscosity combination, a series of torque measurements were made. In preparation, the fluid was pumped into the pressure tank, the air pressure regulator was adjusted for the desired flow rate, and the weigh tank drain valve was closed. The fluid flow was started, the rotor was turned on, the system was operated until steady-state was assured, and the following readings were taken:

a. Room temperature.

b. Fluid level below the top of the rotor.

c. Rotor speed.

d. Fluid flow rate - (by measuring the time interval for an incremental weight of fluid to flow into the weigh tank).

e. Drive force on dynamometer.

At the same time, a fluid sample was collected as it ran into the weigh tank, and the fluid viscosity and temperature were measured.

The same preparations and start-up procedure was followed for the heat transfer measurements. When the recording potentiometer showed steady-state, the following readings were taken:

a. Room temperature.

b. Rotor speed.

c. Fluid flow rate - (as above)

d. Potentiometer reading in millivolts for each of the thermocouples, progressing from couple number 1 through number 8.

The same procedure as above was followed in determining the fluid viscosity.

CHAPTER III

RESULTS

The results of the experimental work show that type A blades produce the scraping and mixing effects that are necessary to obtain the optimum heat transfer rates. The rotor speed, the fluid viscosity, and the number of blades all influence the rotor driving torque requirements. A torque equation to show the relationship of the variables is derived from the measurements. The improvement in heat transfer rates with scraping is evaluated. The detailed results of the three phases are discussed separately.

Visual Observations

The first visual observations were made with no blades on the rotor. They confirmed the design calculations for smooth concentric cylinders that both rotational and axial flows are laminar within the defined limits of rotor speed and viscosity.

Two type A blades were installed on the rotor, and the fluid motion was observed for the entire series of rotor speed and fluid viscosity combinations. In all cases, the fluid responded to the blade action in substantially the same way. An approximate absolute velocity profile of the fluid in the annulus with type A blades is shown in Figure 13. That fluid right next to the stator surface remains at rest, and that fluid right next to the rotor surface moves at rotor speed. The dotted line indicates the fluid velocity distribution if no blades were on the rotor. Superimposed on this pattern is another motion caused by the pumping action of the blades. The resultant profile shows that

within the annular space the maximum fluid velocity is higher than the rotor speed. It is estimated that this maximum velocity is about 1.5 times rotor speed.

Because the quantity of fluid between two blades remains a constant and some of the fluid moves faster than the rotor, it follows that some of the fluid has a relative motion opposite to the direction of rotation of the rotor. The relative motion of the fluid with respect to the blade is shown in Figure 14. It is this action that produces the mixing effect that is required to realize the potential heat transfer rates in a scraped-surface exchanger. As the scraper removes the heated or cooled film at the stator surface, it causes this material to flow toward the rotor surface and move at the higher velocity. On the opposite side of the blade, the fluid that was near the rotor surface is directed to the stator surface. Thus, after each time a scraping blade passes, fluid at the bulk temperature is presented to the heat transfer surface and the temperature gradient at the interface is a maximum. The action described above and illustrated in Figures 13 and 14 is substantially the same with 1, 2, or 4 type A blades installed on the rotor.

The ends of the blades are not covered, shielded, or baffled so the fluid is free to respond to the blade pressures. Figure 15 illustrates the motion of the fluid at the top end of the blades. Because the fluid essentially bypasses the blade and escapes from between two blades, the circumferential flow pattern described above is disturbed. The fact that there is a low pressure area at the blade trailing edge is evident in the flow streamlines, and in addition, any air bubbles in the fluid will accumulate into an air pocket at this trailing edge near the

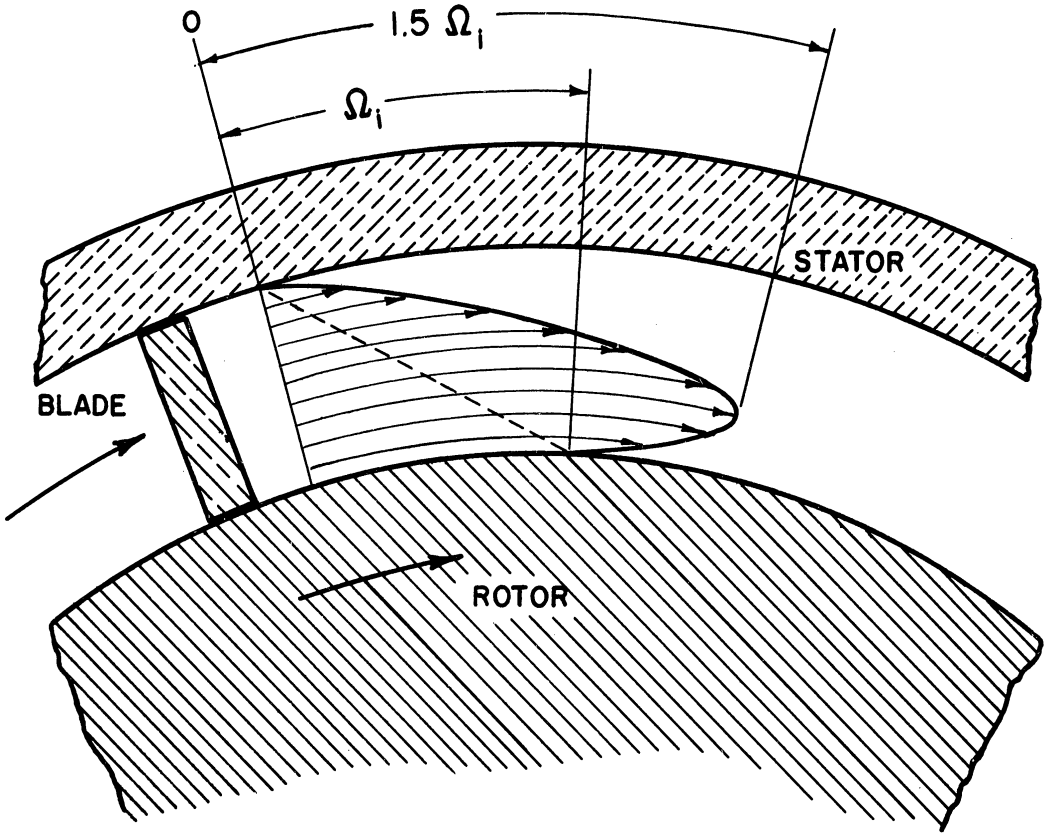

Figure 13. Approximate Velocity Profile of Fluid in Annulus with Type A Blade.

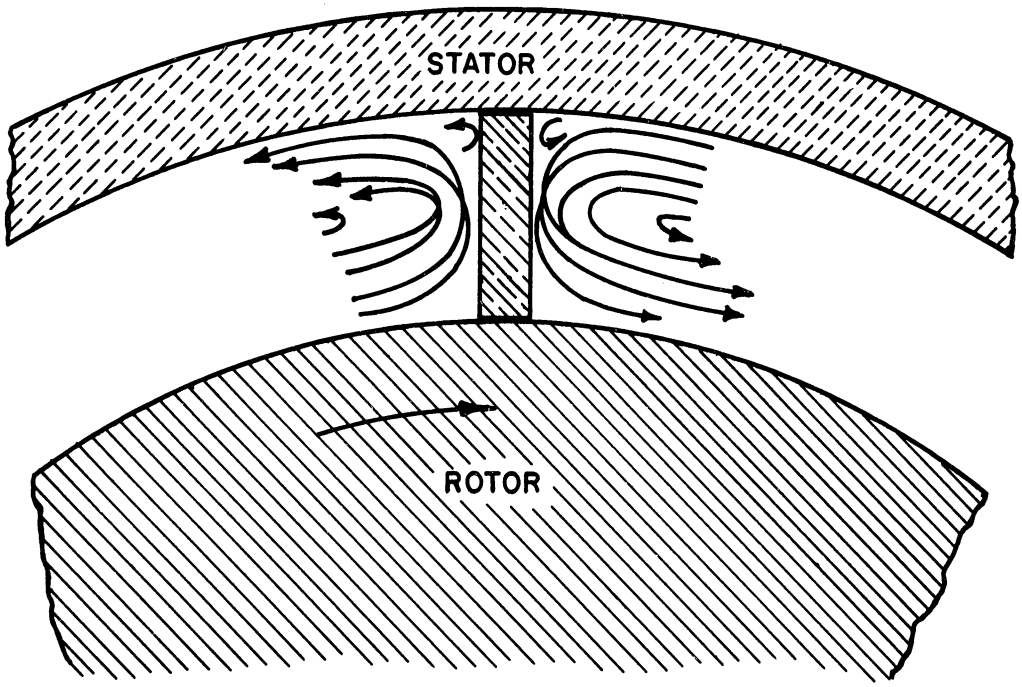

Figure 14. Relative Motion of Fluid with Respect to Type A Blade and Rotor.

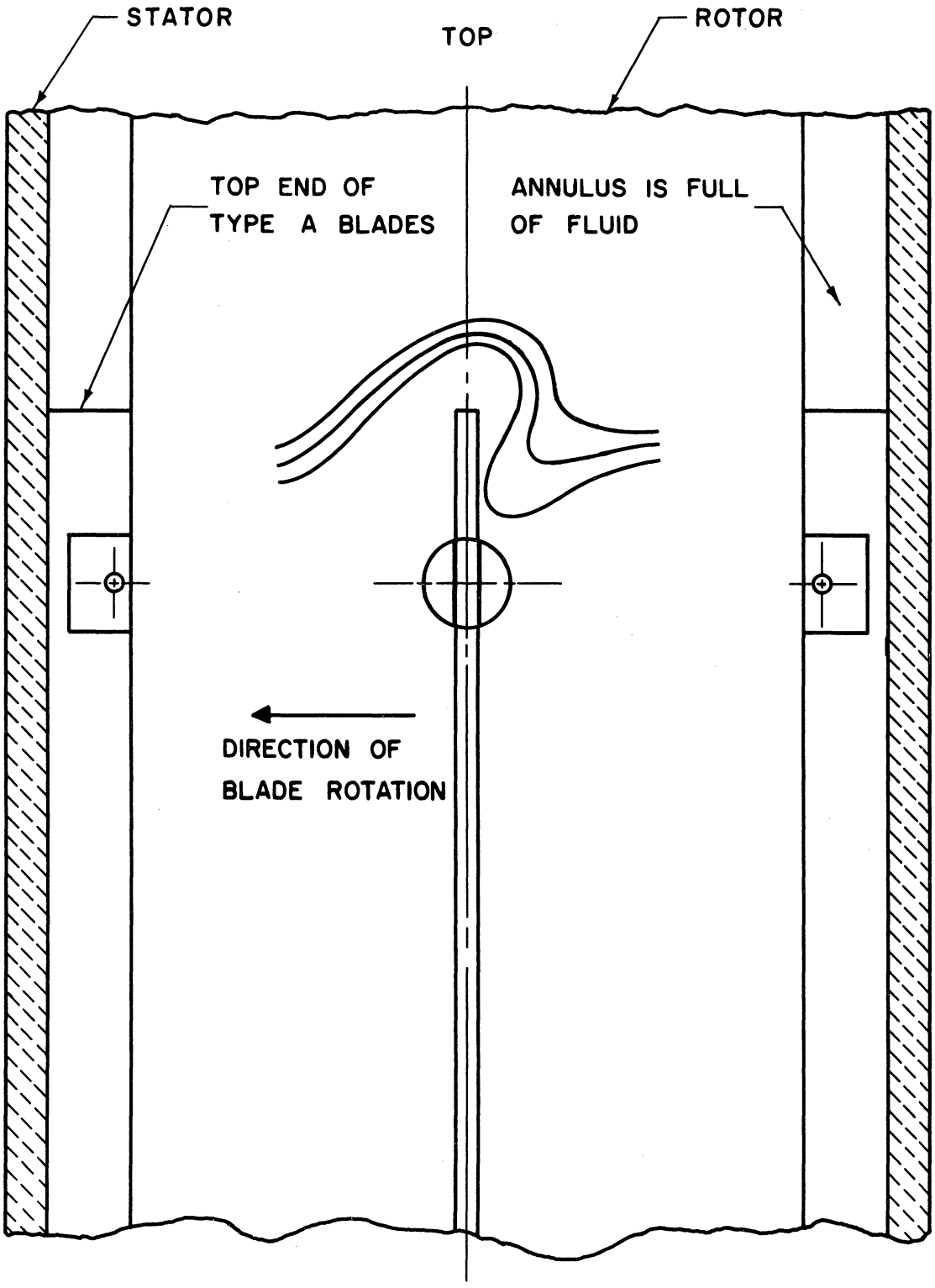

Figure 15. Streamlines in Fluid Showing Blade End Effects with Type A Blade.

top of the blade. The end effects are less apparent as the number of blades increase from 1 to 4.

A further measure of the pressure gradient between the trailing edge of one blade and the leading edge of another was possible by operating the unit partially full of fluid. Under these conditions, the fluid level is responsive to the blade pressure. The difference between the fluid level at the leading edge of one blade and the fluid level at the trailing edge of the next blade was measured as follows:

Fluid Viscosity Centipoises	Rotor Speed rpm	Difference in Fluid Level Inches
6900	32.	15.25
2000	32.	7.79
2000	60.	12.00

At higher speeds and higher viscosities, the fluid would overflow the top of a blade, meaning that the pressure gradient was greater than 16-5/8 inches.

When type B blades were installed on the rotor, the fluid motion was changed considerably. As is illustrated in Figure 16, the velocity profile approaches that of fluid in an annulus between smooth, concentric, rotating cylinders. The relative motion of the fluid with respect to a blade is shown in Figure 17. Although the blade scrapes the fluid from the stator, or heat transfer surface, this fluid which has been heated or cooled is not mixed with the remaining bulk fluid. The streamlines are compressed and the velocity of fluid is increased when a blade passes, but there is substantially no mixing. That fluid

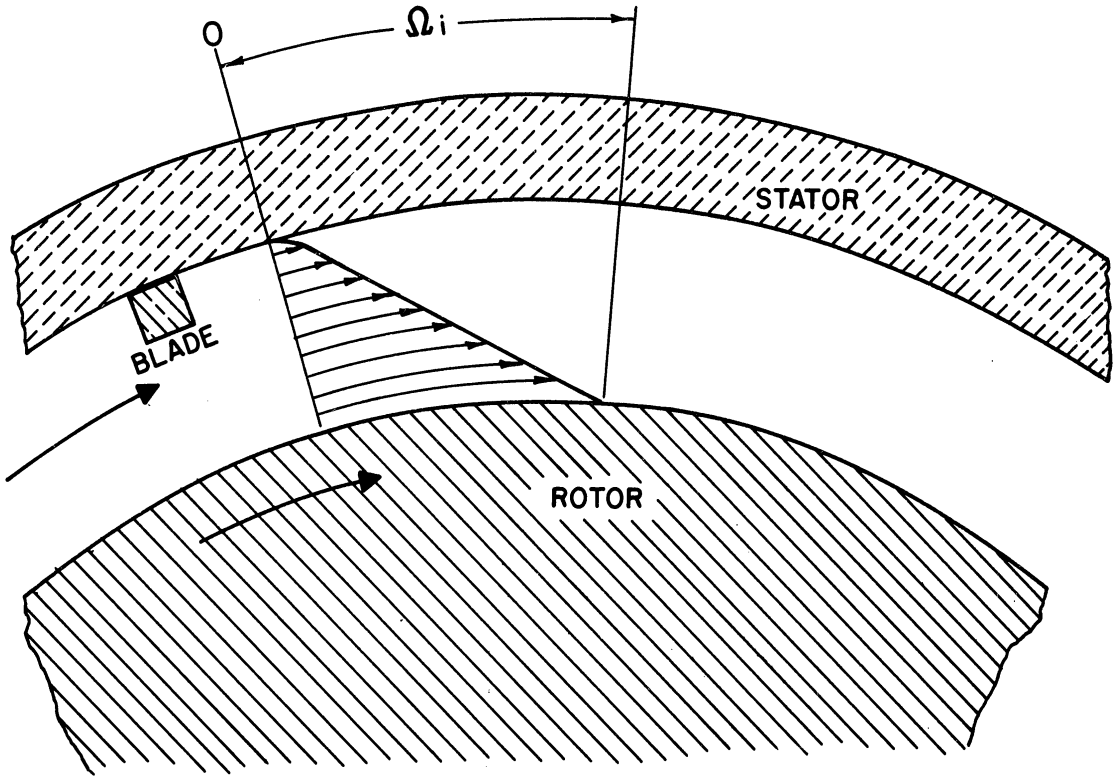

Figure 16. Approximate Velocity Profile of Fluid in Annulus with Type B Blade.

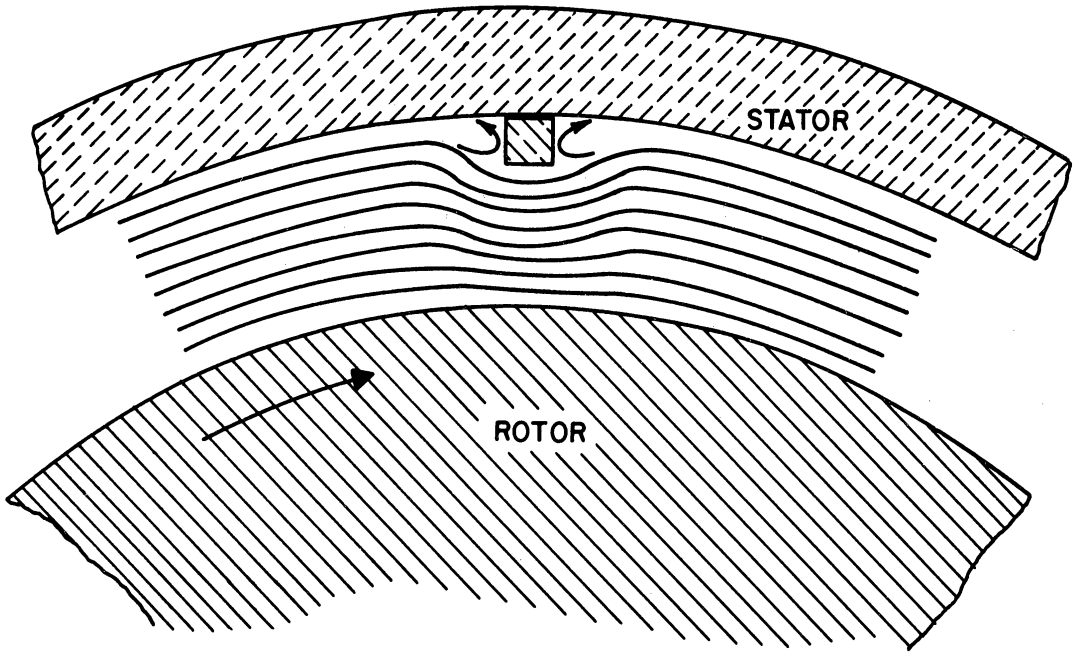

Figure 17. Relative Motion of Fluid with Respect to Type B Blade and Rotor.

which was right next to the scraped surface returns to that surface, and the remainder of the fluid is undisturbed. Axial flow does nothing to improve the mixing, because these streamlines also stay in their same relative position. Thus the type B blade does not fulfill one of the basic requirements, that the heated or cooled scraped film be mixed with the bulk fluid and new bulk fluid be presented to the heat transfer surface.

Torque Measurements

The complete results of the torque measurement studies are given in Table I in the Appendix. The fluid viscosity, column E, is the average of several measurements made at different shear rates on a single sample collected from the fluid flowing out of the annulus. The active rotor length, column H, is the height of the fluid on the rotor determined by subtracting the exposed length of the rotor from the total rotor length.

For each given combination of blades, rotor speed, and fluid viscosity, the fluid level was adjusted to the bottom of the rotor, and the torque was measured. This "friction" torque is that torque required to turn the rotor because of the following factors:

a. bottom bearing friction,

b. blade drag on the scraped surface,

c. fluid action of the bottom end of the rotor.

For each run shown in Table I, the friction torque is subtracted from the total torque reading to give the observed torque, column I. Because the blades are only 16-5/8 inches long, the torque readings for all runs

are reduced to the equivalent torque for a rotor 16-5/8 inches long. Using the modified Reiner and Riwlin equation, Equation (3), and the rotor dimensional factor from Figure 3, the torque requirements for a smooth rotor with length in excess of 16-5/8 inches are calculated. This calculated torque is subtracted from the observed torque (column I) to give the adjusted torque of column J.

Because of the large number of observations and the interdependence of the variables, an attempt was made to fit a single equation to the data, making use of a digital computer. Westervelt's[16] stepwise regression program with simple learning was used to obtain the equation. The input data were the number of blades (column B), the fluid viscosity (column E), the rotor speed (column G), and the adjusted torque (column J). Only those data for the type A blade were used. It was requested that torque be expressed as a function of speed, viscosity, and number of blades.

The computer determined coefficients and evaluated the sum of terms of power functions of the variables and derived the following equation on its pass number 5 after 15 steps:

$$\begin{aligned} T' = {} & 3.61\, n'\mu' + 8.66\, n'\mu' B^{1/2} - 0.11\, n'\mu' B^{3} - 1.05\, n'^{-1/4}\mu'^{1/5} B^{-6} \\ & + 4.15\, n'^{4} B^{1/2} - 3.04\, \mu'^{-3} B^{4} - 2.80\, n'^{4}\mu'^{1/2} B^{1/3} \\ & - 0.024\, n'^{-1/4}\mu'^{-1/5} B^{6} - 7.88 \times 10^{-9}\mu'^{5} B^{5} \\ & + 1.41\, n'^{1/3} B^{3} + 0.43\, n'^{-1/4}\mu'^{1/4} B^{3} \end{aligned} \qquad (6)$$

Scaling factors in the above equation are

Speed x 10^{-2} (rpm)

Viscosity x 10^{-3} (centipoises)

B as observed (number of blades)

T' as observed (inch pounds)

With the computer, the predicted torque was calculated from the equation and compared with each data point. This was done to evaluate the deviation of the individual data points from the fitted curve. Runs 25 through 32 had a small absolute deviation but a percentage deviation of up to 50% in some cases. In these runs, the friction torque was almost twice the value of the adjusted torque, so a slight error in observations could easily reflect the deviation noted.

The computer indicated that run number 153 had the largest deviation (37.0 inch pounds, 33.1%). Upon reference to the original observation sheets, it was noted that there was considerable entrained air in the viscosity sample, and that the viscosity reading was probably in error.

The computed torque for run number 173 was 12.08 inch pounds high (4.8%), but again, there was reason to question the viscosity reading because there had been some mixing of solutions during a change over, and the sample may not have been representative. Errors for run 281 (2.56 inch pounds, 16.6%) and run 282 (.93 inch pounds, 6.7%) were also high, but the original observation sheets showed that the readings were changing during the runs and that the system was not operating in steady-state.

The fitted curve (including the runs discussed above) had an absolute standard error of 4.70 inch pounds, and a coefficient of determination of 0.998, showing that it was an accurate representation of the data.

The large number and unconventional form of the terms of Equation (6) make an analysis with respect to physical occurrences very difficult. However, when B = 0 (smooth rotor), the equation reduces to

$$T' = 3.61\, n'\mu'$$

Introducing the scaling factors, and dividing both sides by $n'\mu'$, it becomes

$$\frac{T'}{n'\mu'} = 3.61 \times 10^{-5} \tag{7}$$

where

T' = torque in inch pounds

n' = rpm

μ' = viscosity in centipoises

If the dimensional factor for a smooth rotor 16-5/8 inches long (19.52 in^3) is introduced into Equation (3), it is

$$\frac{T'}{n'\mu'} = 3.66 \times 10^{-5} \tag{8}$$

Thus there is excellent agreement between the theoretical equation for a smooth rotor and that portion of Equation (6) which applies to a smooth rotor, indicating that both the data and the curve fitting technique are valid.

A more conventional method of analysis of these data can be made with a dimensional analysis study, again using a digital computer to determine the coefficients and the exponents of the dimensionless groups. The following are considered to be significant variables:

$$\text{Torque} = T - \frac{ML^2}{\theta^2}$$

$$\text{Viscosity} = \mu - \frac{M}{L\theta}$$

No. of blades = B - dimensionless

$$\text{Speed of blade at scraped surface} = V - \frac{L}{\theta}$$

Radial clearance between rotor and stator = d - L

Density of fluid = $\rho - \frac{M}{L3}$

Length of active rotor = ℓ - L

Axial velocity is not included as a variable because the work of Goldstein[4] and others show that within the laminar flow range, axial and rotational flows are independent.

These can be arranged in dimensionless groups as

$$\frac{T}{d3\rho V2} = \gamma'(\frac{\mu}{\rho Vd})^a(B)^b(\frac{\ell}{d})^c \qquad (9)$$

From the analysis of the visual observations, it is evident that the torque is a function of two factors, i.e., (1) that torque required to turn a smooth rotor, and (2) that torque required to turn the rotor because of the blade effects. In order to separate these effects, Equation (9) is written

$$\frac{T}{d3\rho V2} = \gamma_1'(\frac{\mu}{\rho Vd})^{a1}(\frac{\ell}{d})^{c1} + \gamma_2'(\frac{\mu}{\rho Vd})^{a2}(B)^b(\frac{\ell}{d})^{c2} .$$

Substituting

$$V = 2\pi R_o n$$

$$\frac{T}{4d^3\rho\pi^2 R_o^2 n^2} = \gamma_1'(\frac{\mu}{2\pi R_o n\rho d})^{a1}(\frac{\ell}{d})^{c1} + \gamma_2'(\frac{\mu}{2\pi R_o nd})^{a2}(B)^b(\frac{\ell}{d})^{c2}$$

since $\frac{\ell}{d}$ is constant for this apparatus, there is no opportunity to evaluate C_1 or C_2, so let

$$\gamma_1'(\frac{\ell}{d})^{c1}\frac{4\pi^2}{2\pi} = \gamma_1$$

and

$$\gamma_2'(\frac{\ell}{d})^{c2}\frac{4\pi^2}{2\pi} = \gamma_2$$

then

$$\frac{T}{d^3\rho R_o^2 n^2} = \gamma_1\left(\frac{\mu}{R_o n\rho d}\right)^{a_1} + \gamma_2\left(\frac{\mu}{R_o n\rho d}\right)^{a_2}(B)^b \qquad (10)$$

From this, the computer program was written to evaluate the best coefficients and exponents in the least squares sense based on the equation

$$\frac{T'}{n'^2} = \alpha_1\left(\frac{\mu'}{n'}\right)^{a_1} + \alpha_2\left(\frac{\mu'}{n'}\right)^{a_2}(B)^b \ . \qquad (11)$$

The values obtained were

$$\alpha_1 = 3.24 \times 10^{-5}$$

$$\alpha_2 = 1.01 \times 10^{-4}$$

$$a_1 = 1.0$$

$$a_2 = 1.0$$

$$b = 0.46$$

Introducing the proper numerical conversion factors, this solution is written into Equation (10) as

$$\frac{T}{d^3\rho R_o^2 n^2} = 2.41 \times 10^4\left(\frac{\mu}{R_o n\rho d}\right) + 7.51 \times 10^4\left(\frac{\mu}{R_o n\rho d}\right)(B)^{0.46} \qquad (12)$$

all in consistent units. The questionable data were not included in this calculation.

To indicate the spread of the data, $\frac{T'}{n'^2}$ was calculated and compared with corresponding observed values. With but few exceptions, the calculated values are well within $\pm$ 10% of the observed readings.

For a smooth rotor, Equation (11) can be written

$$\frac{T'}{n'^2} = 3.24 \times 10^{-5}\ \frac{\mu'}{n'}$$

or

$$\frac{T'}{n'} = 3.24 \times 10^{-5} \qquad (13)$$

This compares with the theoretical Equation (8). It is noted that agreement is not as good as with the equation derived by the stepwise regression method for the zero blade condition.

The visual studies showed that type B blades would not give the mixing effect required to achieve maximum heat transfer rates, so the torque measurements with type B blades were not extensive. An analysis of the data in runs 309 through 354 yields the equation

$$T = 8.8\ \mu\pi\ \frac{\Omega_i}{1/R_i^2 - 1/R_o^2} \qquad (14)$$

The torque calculated with this equation is in excellent agreement with the observed adjusted torque. However, it should be emphazized that the effect of the number of blades was not investigated, and this equation is based on only 2 type B blades.

Heat Transfer Measurements

The heat transfer measurements were made to demonstrate the improvement in heat transfer rates that results when properly designed scraping blades are added to a smooth rotor operating within a concentric heat transfer cylinder. Two independent thermal effects are noted in the heat transfer run, as follows:

a. the energy added to the fluid by the mechanical effects of the rotating rotor and blade system,

b. the energy added to or removed from the fluid because of heat transmission at the heat transfer surface (scraped surface).

The way the temperature of the fluid responds to these thermal effects is different for various conditions. The temperature profile of

the fluid as it passes through the apparatus illustrates its response characteristics for the following three conditions:

a. Energy is added to the fluid because of mechanical effects alone. Figure 18 shows this as a linear temperature increase of the fluid as it passes through the apparatus in the annulus with the rotor and blade system rotating. It is recognized that end effects, blade length, and other factors cause the profile to be other than a straight line, but the assumption is approximately correct because the influence of these factors is small.

b. During heating, energy is tranferred from the scraped surface to the fluid and, at the same time, energy is added to the fluid because of the mechanical effects. Figure 19 shows the fluid temperature profile in relation to the heat transfer surface temperature. The components which contribute to the total temperature rise of the fluid are broken down and detailed on the drawing.

c. During cooling, energy is tranferred from the fluid to the scraped surface, and, at the same time, energy is added to the fluid because of the mechanical effects. Figure 20 shows the fluid temperature profile in relation to the heat transfer surface temperature for these conditions. As above, the components which contribute to the fluid temperature change are detailed.

The location of the significant thermocouples is also noted on these drawings. Points 1 and 2 are in the fluid just as it enters the

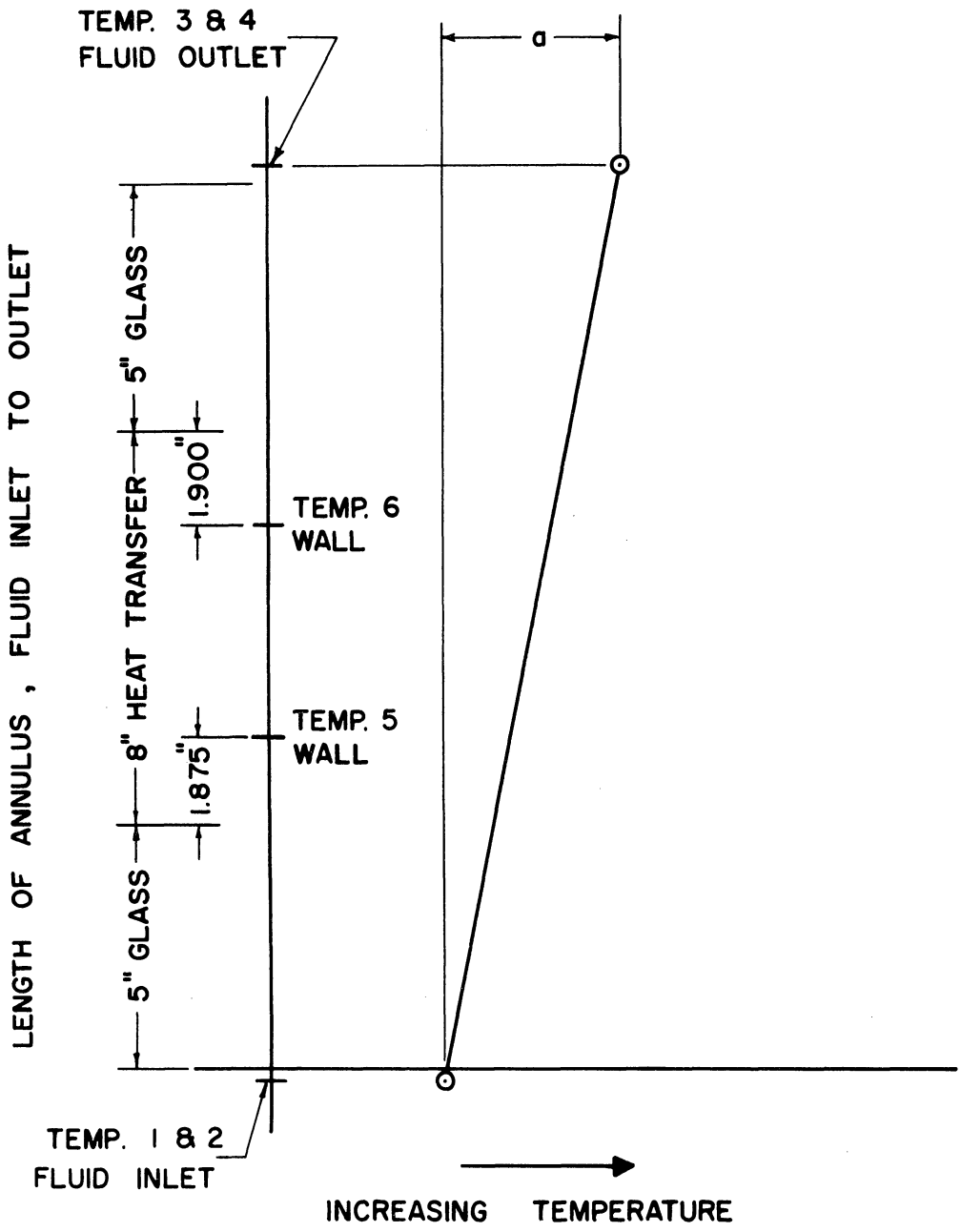

a = total fluid temperature rise - due only to input of mechanical effects

Figure 18. Temperature Profile with Only Mechanical Effects.

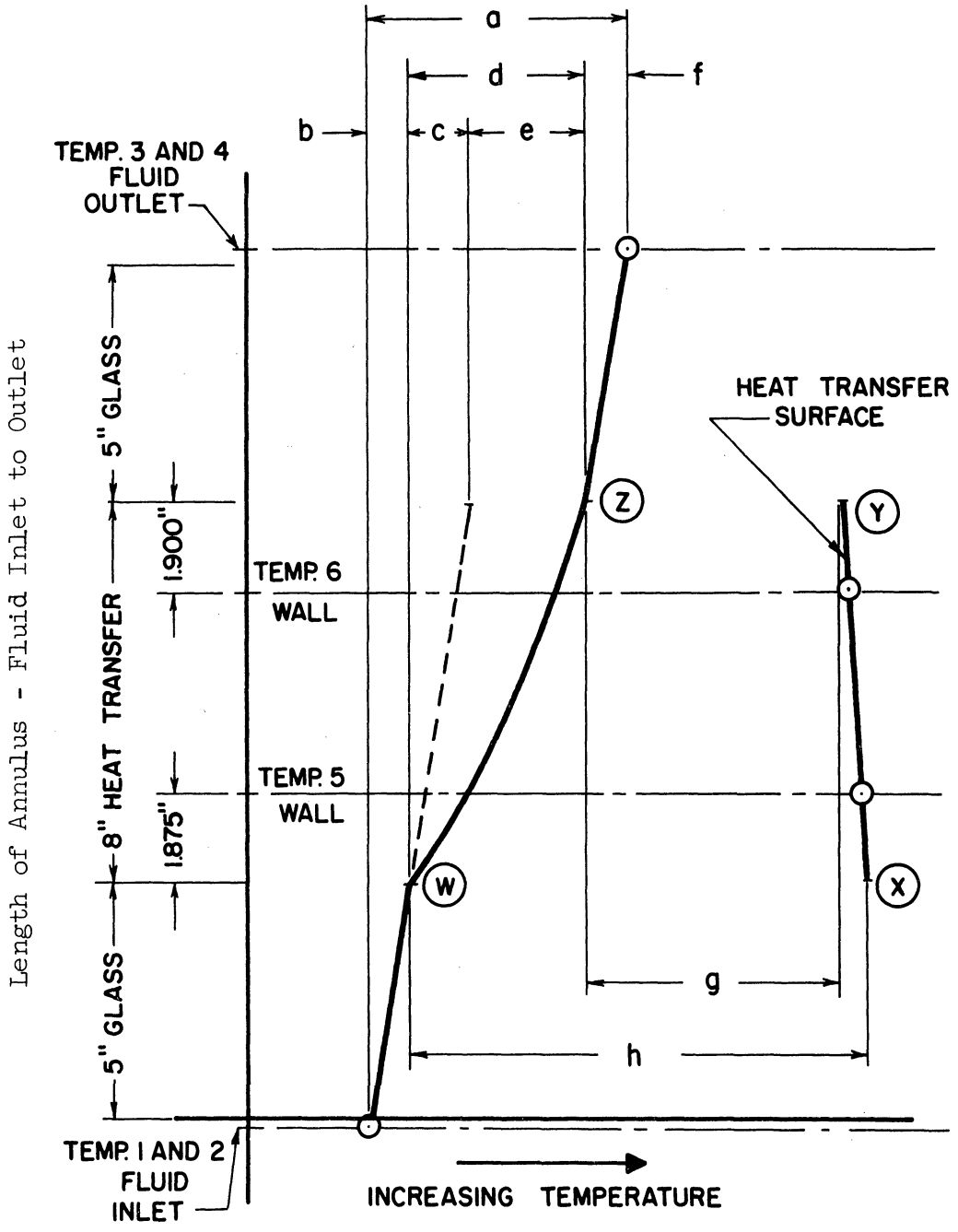

a - total fluid temperature rise
b - fluid temp. rise due to mech. effects before heating zone
c - fluid temp. rise due to mech. effects in heating zone
d - total fluid temp. rise in heating zone
e - fluid temp. rise due to heat transfer at surface
f - fluid temp. rise due to mech. effects after heating zone
g - outlet temp. difference - wall to fluid
h - inlet temp. difference - wall to fluid

Figure 19. Temperature Profile - Heating plus Mechanical Effects.

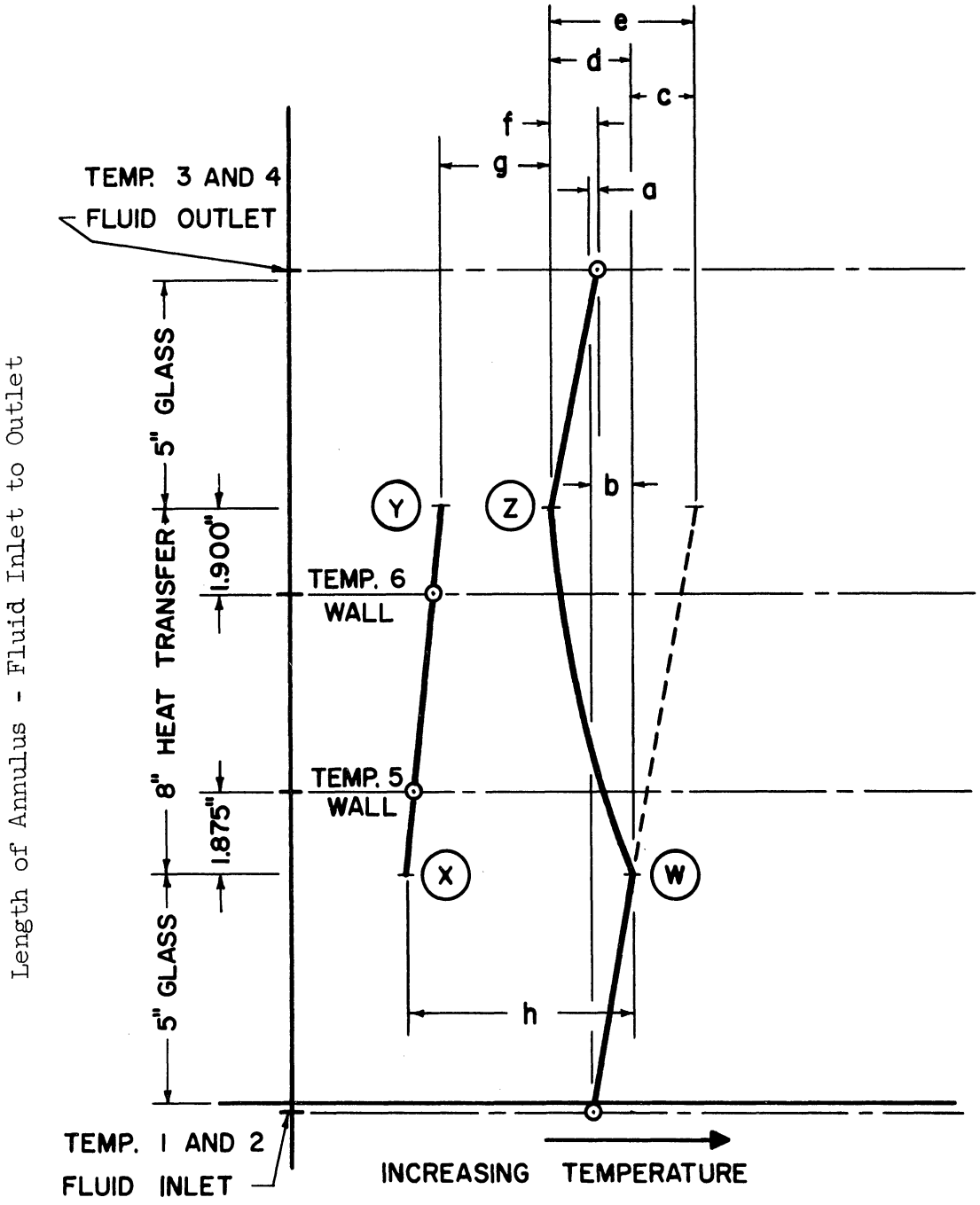

a - total fluid temperature rise
b - fluid temp. rise due to mech. effects before cooling zone
c - fluid temp. rise due to mech. effects in cooling zone
d - total fluid temp change in cooling zone
e - fluid temp. change due to heat transfer at surface
f - fluid temp. rise due to mech. effects after cooling zone
g - outlet temp. difference - wall to fluid
h - inlet temp. difference - wall to fluid

Figure 20. Temperature Profile - Cooling plus Mechanical Effects.

annulus, and points 3 and 4 are in the fluid just as it leaves the annulus. Points 5 and 6 are at the wall of the scraped surface, but at a distance from the entrance and exit ends of the heat transfer portion of the stator. In this location, tube end effects (conduction to insulating spacers) will not influence the reading. If it is assumed that the temperature gradient is linear along the length of the scraped surface, then the temperature of this surface at entrance and exit can be calculated by extrapolation of the temperature profile line through points 5 and 6.

To evaluate a coefficient of heat transfer at the scraped surface, it is necessary to separate the mechanical effects from the purely heat transfer effects. In order to measure the mechanical effects, two series of runs were made with no heat transfer. Table II in the Appendix is a summary of these data for the rotor with 2 and 4 type A blades with two solutions made with 77.5% and 83.0% Ucon. Table III in the Appendix is a summary of the data for the other series for a smooth rotor with a solution made with 83.0% Ucon.

To correlate these data, a dimensional analysis of the mechanical effects alone is made. It is assumed that the energy input to the fluid is a function of the following:

$$\text{Energy into fluid} = f(\mu, V, \rho, d, \ell)$$

also

$$\text{Energy input to fluid} = W\, C_p\, \Delta t_{\text{mech}}$$

where

W = Axial flow rate - lbs/hr

C_p = Specific heat - Btu/lb; °F

Δt_{mech} = Temperature rise (a, Figure 18) - °F

These variables can be arranged in dimensionless groups as

$$\frac{[WC_p\ \Delta t_{mech}]g_c J}{V^3 \rho\ d^2} = \alpha\left(\frac{\mu}{Vd\rho}\right)^a \left(\frac{\ell}{d}\right)^b$$

Substituting

$$V = 2\pi R_o n$$

This becomes

$$\frac{[WC_p\ \Delta t_{mech}]g_c J}{(2\pi R_o n)^3 \rho d^2} = \alpha\left(\frac{\mu}{2\pi R_o n \rho}\right)^a \left(\frac{\ell}{d}\right)^b$$

For the apparatus used in these studies, the physical dimensions do not change. Grouping all constants, the equation can be written as

$$\frac{WC_p\ \Delta t_{mech}}{n'^3} = \alpha_1\left(\frac{\mu'}{n'}\right)^a \quad . \tag{15}$$

These quantities are tabulated in Table II and III with the data, and are plotted in Figures 21 and 22. It is not necessary to determine the numerical values of the exponents and coefficients, because the curves are used directly in later calculations.

It is evident from the temperature profiles, shown in Figures 19 and 20, that a heat transfer coefficient must be calculated from only that temperature change of the fluid which occurs because of heat transfer at the scraped surface. This is represented by the temperature change "e" on Figures 19 and 20, and the symbol Δt_{net}. It is calculated by subtracting the temperature rise due to mechanical effects from the total temperature change of the fluid. On Figures 19 and 20 this can be represented by

$$\Delta t_{net} = e = a\text{-}b\text{-}c\text{-}f$$

where the letters are defined on the figures.

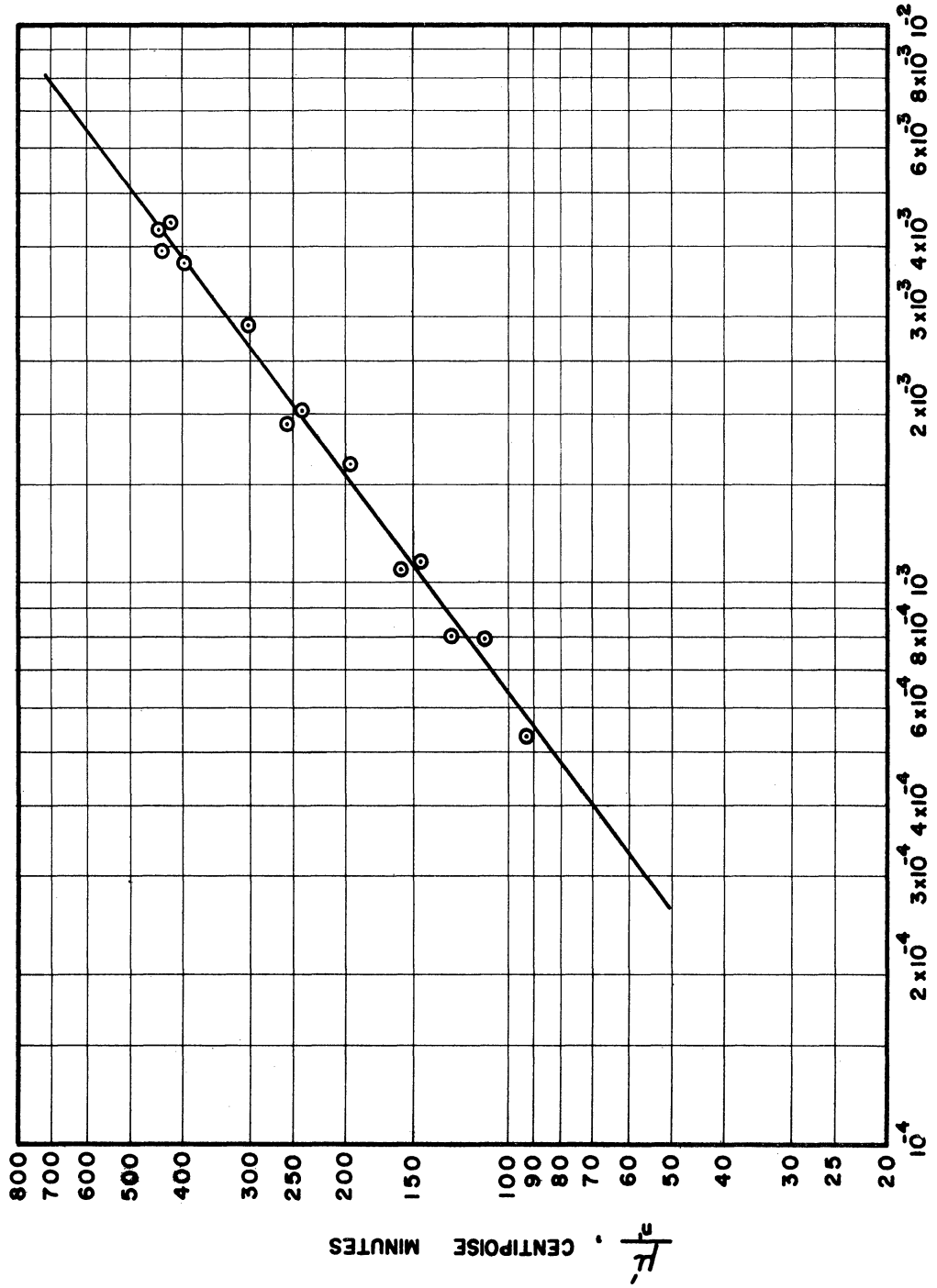

Figure 21. Plot of Significant Groups for Mechanical Input of Rotor and Blades.

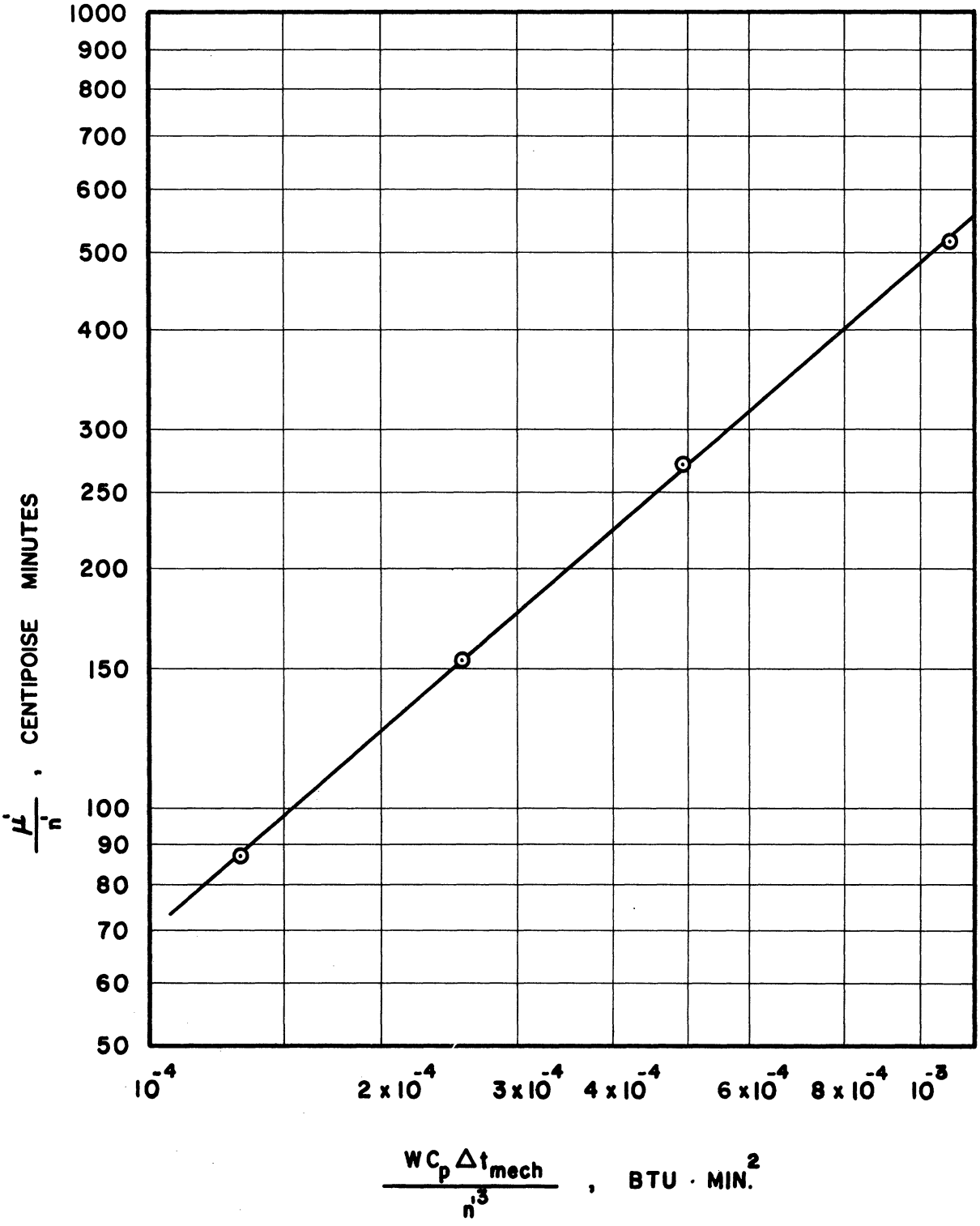

Figure 22. Plot of Significant Groups for Mechanical Input with Smooth Rotor.

For each run, the temperature rise due to the mechanical effects, Δt_{mech}, is determined from Figures 21 and 22. The ratio $\frac{\mu'}{n'}$ is used to find $\frac{WC_p \Delta t_{mech}}{n'3}$ on the graph, and Δt_{mech} calculated from this value.

It is recognized that the mechanical effects were measured under approximately adiabatic conditions, and then were used with heat transfer measurements. Small temperature differences in the fluid were maintained so that this approximation had little influence on the results.

It is also necessary to know the temperature difference between the exit and entrance ends of the scraped surface and the fluid. The temperatures at the ends of the scraped surface (x and y - Figures 19 and 20) are calculated by graphically extrapolating wall temperatures 5 and 6 to the ends of the tube, assuming linear distribution. The temperature of the fluid at w (Figures 19 and 20) is calculated by adding (5/18) (Δt_{mech}) to the fluid inlet temperature (average of 1 and 2). The temperature of the fluid at z (Figures 19 and 20) is calculated by subtracting (5/18) (Δt_{mech}) from the fluid outlet temperature (average of 3 and 4). Then temperature differences g and h (Figures 19 and 20) can be used to calculate the log mean temperature difference.

Table IV is a summary of the heat transfer data and the calculated heat transfer coefficient for the apparatus with 2 and 4 type A blades attached to the rotor. Table V contains similar data for a smooth rotor. The analysis of these data is simplified with an equation derived by dimensional analysis.

For the condition with type A blades, it is assumed that

$$h = f(C_p, k, \rho, V, B, R_o, \mu, d)$$

where

h = film coefficient at scraped surface, Btu/hr; ft^2; °F

C_p = specific heat of fluid, Btu/lb; °F

k = thermal conductivity of fluid, Btu/lb; ft^2; °F/ft

ρ = density of fluid, lbs/ft^3

V = speed of blade at scraped surface, ft/hr

B = number of blades

R_o = radius of stator bore, feet

μ = viscosity of fluid, lb/hr; ft

d = annular gap, ft

These variables can be arranged in dimensionless groups to give the equation

$$\frac{hd}{k} = \alpha \left(\frac{C_p\mu}{k}\right)^a \left(\frac{Vd\rho}{\mu}\right)^b \left(\frac{d}{R_o}\right)^c (B)^d$$

If the blade thickness is neglected, the annular passage between two blades can be considered to have a length factor $\frac{2\pi R_o}{B}$. The last two groups can be combined as $\left(\frac{dB}{2\pi R_o}\right)$ which is a $\left(\frac{d}{L}\right)$ factor. Now the Nusselt number is proportional to the product of a Prandtl number, a Reynolds number, and a $\left(\frac{d}{L}\right)$ ratio. These are usually combined into a Graetz number for laminar flow. Making this combination and substituting $V = 2\pi R_o n$ the equation becomes

$$\frac{hd}{k} = \alpha \left(\frac{C_p\ d^2\rho\ \ nB}{k}\right)^a$$

Substituting $nB = s$, the correlating equation is

$$\frac{hd}{k} = \alpha \left(\frac{C_p\ d^2\rho\ s}{k}\right)^a \qquad (16)$$

These calculated groups are tabulated in Table IV with the data, and plotted in Figure 23. The measured temperatures are to the nearest 0.1 °F, but small differences in the readings make large changes in the heat transfer coefficient. All of the readings taken during a run are included to show the spread. The average value of h is used to calculate $\frac{hd}{k}$. Although there is considerable spread, the slope of the curve, and thus the exponent of $\frac{c\rho sd^2}{k}$ is clearly evident. As the frequency of scraping the surface decreases, the film coefficient approaches the coefficient for a smooth rotor. For conditions where the group $\frac{c\rho sd^2}{k}$ exceeds 3000, the correlating equation is

$$\frac{hd}{k} = 0.104 \left(\frac{C_p \rho s d^2}{k}\right)^{0.62} \tag{17}$$

In a similar manner, the data for a smooth rotor is calculated and tabulated in Table V and plotted in Figure 24. The correlating equation is

$$\frac{hd}{k} = 10.0 \left(\frac{C_p \rho n d^2}{k}\right)^{0.03} \tag{18}$$

where

n = rotor speed in rev/hr

replacing s in Equation (17)

Discussion

If the heated or cooled fluid film is scraped from the heat transfer surface and then returned to the surface, it is obvious that the full advantages of the scraped surface heat exchanger cannot be realized. With very visious fluids, such as used in this work, both rotational and axial flows are laminar and are very stable. As visually observed, a

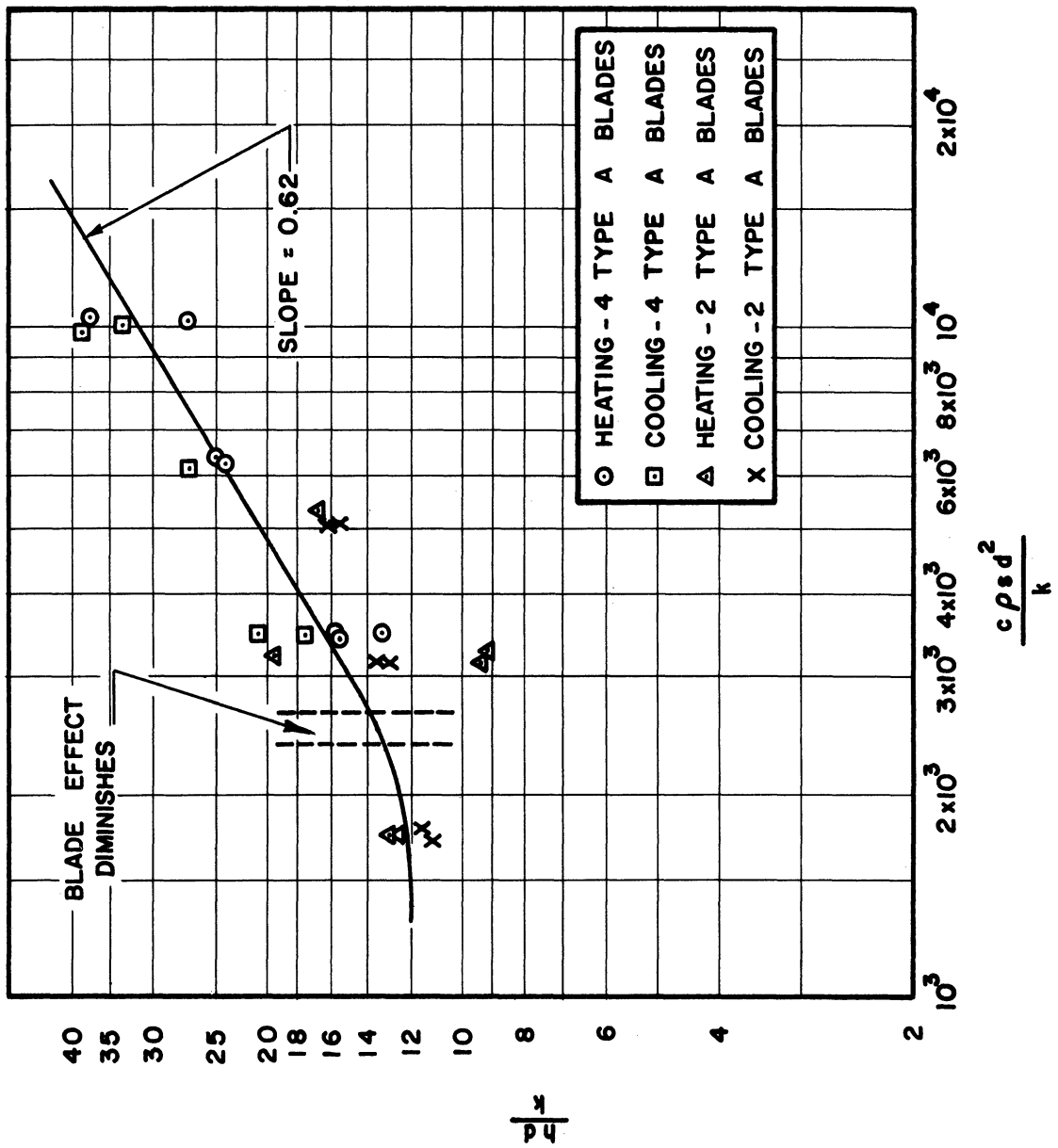

Figure 23. Plot of Dimensionless Heat Transfer Groups.

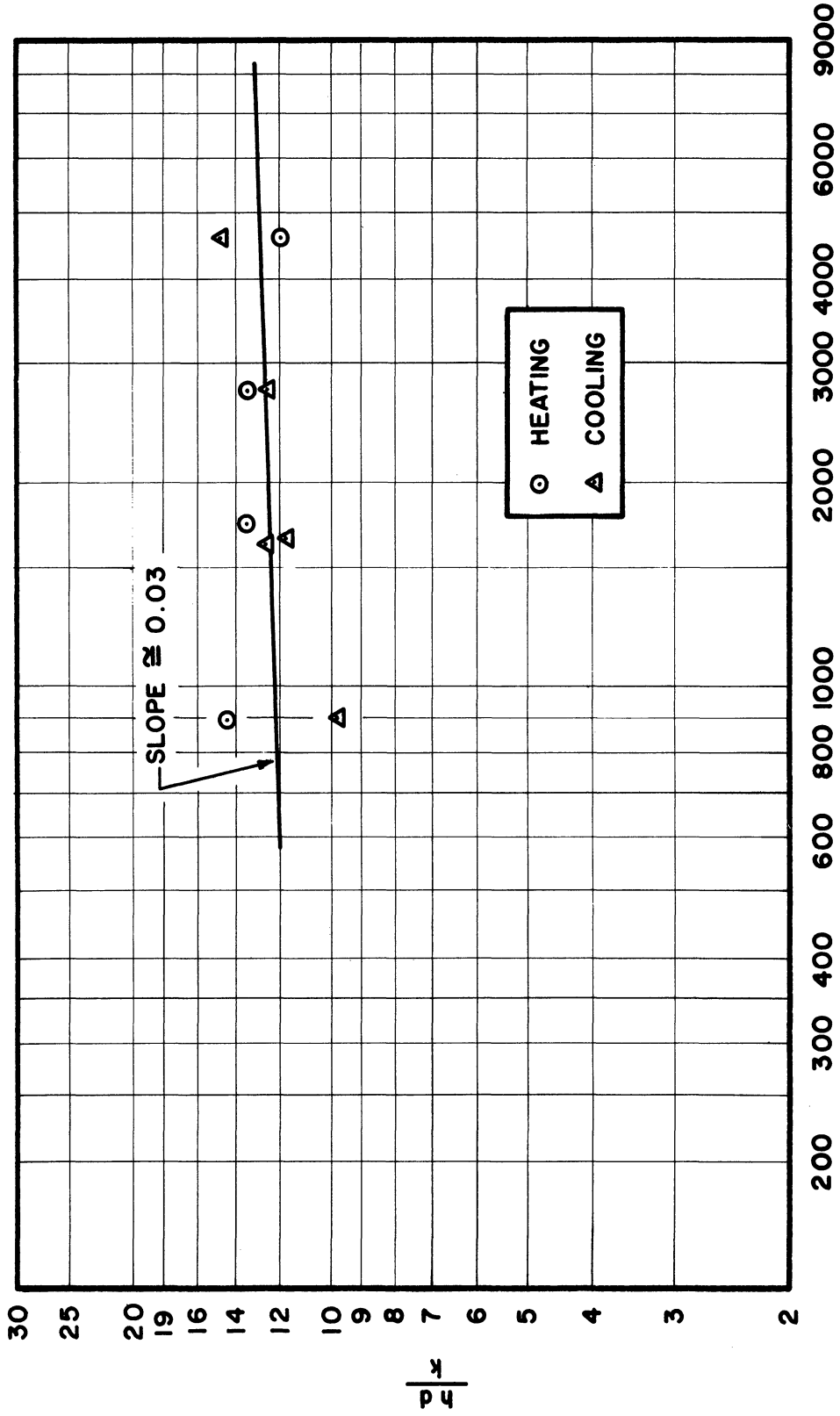

Figure 24. Plot of Dimensionless Heat Transfer Groups - No Blades.

disturbing element such as the type B blade did not change the mode of flow, even though its scraping action is effective. It is necessary that the blade produce forced mixing as well as scrape the surface.

The type A blade accomplishes these objectives. The pressure difference between the leading and trailing edges of the blades is caused by the shear effects in the fluid and by the turning around of the scraped film. This pressure difference "pumps" the fluid within the space between blades where the fluid is trapped. At each end of the closed passage (at the blade faces) the pumped fluid must turn 180°, and mixing is assured. It should be recognized that this mixing is still not complete. There is material right next to the rotor face which may never get to the heat transfer surface.

The springs in the blade mounting attachments exert enough force to move the blades to their outward position. This force is not enough to scrape the surface completely dry, because the Ucon fluid is a lubricant, and its film is tenacious. It is estimated that this film is 0.003" to 0.010" thick, and acts as a lubricant. The presence of this very low velocity fluid does influence the heat transfer film coefficient.

The motion of the fluid with the type A blade is especially significant. There is no known reference in the literature to a blade that completely spans the annulus. Kern[9] recognized that an application of Skelland's[12] equations to fluids in laminar flow would be in error because of the core of unmixed fluid next to the rotor.

In industrial practice, the blades can be mounted in many ways so that they span the annular gap and give the degree of scraping pressure

desired. One possible arrangement is a blade hinged at the rotor so that the action of the fluid holds the blade edge on the heat transfer surface.

An apparent reason for knowing the power requirements is to design the driving machinery. Equally important is the influence of the power input on the net heat transfer effect. For economical reasons it is desireable to keep the power demand as low as possible, consistent with heat transfer performance. In addition, most of the mechanical energy input is added to the fluid, and becomes an additional load on the heat transfer surface in cooling applications. The conclusion is that the heat exchanger should be designed to require the least power in relation to the maximum heat transfer rate.

The equations developed in this work show how speed of rotation and the number of blades affect power demand and the heat transfer rate. Since power is proportional to the product of torque and speed, from Equation (12) it can be shown that

$$\text{power} \propto n^2(1 + B^{0.46})$$

and from Equation (17)

$$h \propto (n)^{0.62}\ (B)^{0.62} \quad .$$

From these equations it is apparent that the addition of more blades causes the heat transfer coefficient to increase at a faster rate than the power requirements. Increasing speed causes the power to increase faster than the heat transfer coefficient. For a given heat transfer coefficient, physical dimensions, fluid, and frequency of scraping, the best arrangement is the largest practical number of blades operating at the lowest speed.

In the only literature dealing with power consumption of a scraped-surface heat exchanger, Skelland and Leung[13] have made a dimensional

analysis of the problem and evaluated the exponents and coefficients experimentally. Their data are not consistent, so they suggest two possible equations and indicate the need for additional work. Except for the fact that they did not consider the annular gap a significant parameter, the dimensionless groups are the same as in this work.

An explanation for the poor correlation of their data can be found in an analysis of the mode of rotational fluid flow. The blades on their rotor did not span the annular gap, so there is some fluid next to the rotor that is not in the path of the blade. If a Taylor number and a critical Taylor number are calculated for a dimensionally similar smooth rotor apparatus and fluid conditions, it can be shown that for some runs the Taylor number is less than critical, and for some greater. For the one condition, there will be no Taylor vortices, and the core fluid will remain in laminar flow rotationally, and will not be mixed with the heated or cooled film. For the other condition, the Taylor vortices do occur and the core fluid is mixed.

In spite of the inconsistencies described above, the exponent applied to the number of blades is in reasonable agreement. They did not consider the zero blade condition, and determined the exponent on the number of blades to be 0.59 or 0.64. If all other parameters which influence torque are considered constant, Equation (12) can be written

$$T = \text{constant } (0.321 + B^{0.46})$$

A comparison is made in the following table:

Number of Blades	$B^{0.59}$	$B^{0.64}$	$(0.321 + B^{0.46})$
2	1.51	1.56	1.70
3	1.91	2.02	1.98
4	2.27	2.43	2.21

The purpose of making the heat transfer measurements in this work was to demonstrate that the heat transfer film coefficient is increased when scraping blades are added to the rotor. A comparison of Figures 23 and 24 clearly shows the effect.

The same comments relative to the mode of rotational flow which were made about the above work of Skelland and Leung[15] apply to that of Skelland, Oliver, and Tooke.[14] Again, in spite of the differences in modes of flow, the effect of the frequency of scraping the surface on the film coefficienct was determined to be of the same order. Assuming all other parameters to be constant, Skelland, Oliver and Tooke found

$$h \propto \text{constant } n^{0.62} B^{0.53}$$

It was found in this work (Figure 24) that

$$h \propto \text{constant } n^{0.62} B^{0.62}$$

The mathematical derivation of Kool[10] was made for an apparatus operating under substantially the same conditions as in this work. He assumes perfect scraping and perfect mixing in setting up a heat balance within the annulus. His solution is given as

$$h_s = h' \left(\frac{2S\pi^{-1/2} + \exp S^2 \operatorname{erfc} S - 1}{S^2 - 2S\pi^{-1/2} - \exp S^2 \operatorname{erfc} S + 1} \right)$$

where

h_s = film coefficient at the scraped surface

h' = film coefficient at jacket fluid surface

$$S = \left(h' \sqrt{\frac{t}{kC_p\rho}}\right)$$

t = time between each scrape

When S has a value of 0.2 to 30,

$$h_s = 1.24\ h'\ S^{-1.03}$$

From this equation, the effect of the frequency of scraping can be expressed as

$$h \propto S^{0.52}$$

which compares with

$$h \propto S^{0.62}$$

determined in this work.

If the film coefficients are calculated using Kool's equation for conditions existing in the experimental work, they are 3 to 4 times higher than those determined experimentally. Kool shows that a residual film of 0.2 mm to 0.5 mm can cause all of this difference. As noted above, the residual film in these experiments could approach this thickness. It is known that the condition of perfect mixing is not attained. Kool also shows the adding scrapers to a smooth rotor will increase the film coefficient by 2 to 4 times.

CHAPTER IV

CONCLUSIONS AND RECOMMENDATIONS FOR FURTHER WORK

A basis for the design of a scraped-surface heat exchanger for viscous fluids with viscosities in the range of 2,000 to 20,000 centipoises has been determined. Specific conclusions from the labroatory observations and measurements of this work are as follows:

1. The required scraping and mixing action will be produced by solid blades attached to the rotor. These blades should span the entire annular gap between the rotor and the stator, so that a complete block to rotational fluid flow occurs at each scraper. The action of this type of scraping blade on the fluid is substantially the same for 1 through 4 blades.
2. Scrapers which are essentially rods will not mix the scraped film with the bulk fluid, and will leave an undisturbed core of fluid next to the rotor.
3. The torque requirements, and thus the power demand, can be calculated from either Equation (6) or (12). Equation (12) is simpler to use and provides almost as good correlation. It is

$$\frac{T}{d^3 \rho R_o^2 n^2} = 2.41 \times 10^4 \left(\frac{\mu}{R_o n \rho d}\right) + 7.51 \times 10^4 \left(\frac{\mu}{R_o n \rho d}\right)(B)^{0.46} .$$

4. The heat transfer film coefficient at the scraped surface shows a significant improvement with the addition of scrapers

to the smooth rotor. The degree of improvement that can be expected can be calculated by comparing the film coefficient calculated from Equation (18) for a smooth rotor with that calculated from Equation (17) for a rotor with blades. These equations are

$$\frac{hd}{k} = 10.0 \left(\frac{c\rho nd^2}{k}\right)^{0.03} \tag{18}$$

$$\frac{hd}{k} = 0.104 \left(\frac{c\rho sd^2}{k}\right)^{0.62} \tag{17}$$

Much additional work needs to be done, because there is very little material in the literature on either the design or the performance of scraped-surface heat exchangers, particularly units for viscous fluids. The following specific recommendations are made:

1. The Taylor number should be used to calculate the mode of rotational fluid flow for a dimensionally similar system with a smooth rotor. Data taken in future work can be classified and properly correlated when the mode of flow is defined.
2. Within the fluid viscosity range of 2,000 to 20,000 centipoises, this work should be extended to higher rotor speeds and more blades.
3. The effects of dimensional changes should be investigated within the limits of commercially practical units. Although the cross sectional area of the annulus must be large enough to avoid a prohibitive axial pressure drop, the influence of the width of the annular gap would be of

interest. The inside diameter of the stator should be as large as possible to obtain maximum heat transfer area per unit length, consistent with a linear scraping speed that will not result in excessive wear.

4. The scraping efficiency of blades should be investigated.

The scraped-surface heat exchanger has a wide field of use where other types of heat exchangers are not effective or economical. In atuomatic and continuous processes, the accurate control of the temperature of viscous components is a necessity. Another application for this type of unit is as an agitated, controlled-temperature chemical reactor. Components can be introduced along the axial length as the base fluid flows through. The heat-transfer jacket can be zoned to provide different temperatures along the length.

The scraped-surface heat exchanger is a versatile mechanical device for use by the chemical process industries. Its industrial application will expand with increased knowledge of design and performance.

APPENDIX

TABLE I

TORQUE MEASUREMENT DATA

A	B	C	D	E	F	G	H	I	J
Run No.	No. of Blades	Blade Type	Axial Flow lbs/min W	Fluid Viscosity Centipoises μ'	Fluid Temp.- °F	Rotor Speed rpm n'	Active Rotor Length Inches	Observed Torque Inch-lbs	Adjusted Torque Inch-lbs T'
1	0	--	4.39	2,133	76.6	164.9	18.733	12.746	11.47
2	0	--	4.39	2,087	76.8	165.6	18.733	12.866	11.57
3	0	--	4.39	2,129	76.6	165.7	18.733	12.866	11.57
4	0	--	4.39	2,126	76.6	166.0	18.733	13.127	11.80
5	0	--	4.44	2,127	76.6	98.5	18.900	9.018	8.06
6	0	--	4.44	2,129	76.6	99.0	18.900	9.018	8.06
7	0	--	4.44	2,120	76.8	98.9	18.900	9.018	8.06
8	0	--	4.44	2,072	76.8	99.0	18.900	9.018	8.06
9	0	--	4.45	1,929	77.7	58.5	18.857	6.252	5.60
10	0	--	4.45	1,993	77.6	58.5	18.857	6.132	5.49
11	0	--	4.45	1,999	77.5	58.5	18.857	6.012	5.39
12	0	--	4.45	2,039	77.4	58.6	18.857	5.891	5.27
13	0	--	4.50	2,131	76.8	32.0	19.012	3.257	2.91
14	0	--	4.50	2,074	76.8	32.0	19.012	3.127	2.79
15	0	--	4.50	2,066	77.0	32.0	19.012	3.127	2.79
16	0	--	4.50	2,055	76.8	32.0	19.012	3.257	2.91
17	0	--	3.96	1,262	73.9	164.0	18.704	7.936	7.14
18	0	--	3.96	1,238	73.9	165.5	18.704	7.816	7.03
19	0	--	3.96	1,238	73.9	165.9	18.704	7.816	7.03
20	0	--	3.96	1,235	73.9	166.6	18.704	7.816	7.03
21	0	--	3.79	1,153	73.8	98.6	18.819	4.930	4.42
22	0	--	3.79	1,220	74.1	98.8	18.819	5.050	4.53
23	0	--	3.79	1,240	73.4	99.0	18.819	4.930	4.42
24	0	--	3.79	1,243	73.5	98.9	18.819	5.170	4.64
25	0	--	3.83	1,368	74.5	58.6	18.900	2.525	2.26
26	0	--	3.83	1,262	74.4	58.9	18.900	2.525	2.26
27	0	--	3.83	1,243	74.3	58.6	18.900	2.525	2.26
28	0	--	3.83	1,235	74.2	58.6	18.900	2.766	2.48
29	0	--	4.06	1,289	74.0	32.0	18.894	1.202	1.08
30	0	--	4.06	1,251	74.0	32.0	18.894	0.962	0.86
31	0	--	4.06	1,241	73.8	32.0	18.894	0.962	0.86
32	0	--	4.06	1,226	73.9	32.0	18.894	0.962	0.86
33	0	--	2.04	14,853	77.9	157.9	18.845	87.534	78.50
34	0	--	2.04	15,153	78.5	158.6	18.845	85.370	76.52
35	0	--	2.04	14,400	79.3	159.0	18.845	85.250	76.50
36	0	--	2.04	13,613	79.8	159.1	18.845	84.288	75.60
37	0	--	2.00	14,280	76.4	96.7	19.013	59.759	53.25
38	0	--	2.00	15,233	76.2	97.1	19.013	58.677	52.30
39	0	--	2.00	15,303	76.7	97.3	19.013	58.316	51.95
40	0	--	2.00	15,107	76.5	97.4	19.013	58.076	51.80
41	0	--	2.21	16,490	74.5	58.3	19.080	34.629	30.83
42	0	--	2.21	16,327	75.0	58.3	19.080	34.509	30.72
43	0	--	2.21	15,940	75.4	58.3	19.080	34.629	30.83
44	0	--	2.21	16,327	75.0	58.2	19.080	34.629	30.83
45	0	--	2.10	15,653	73.9	31.8	19.159	19.599	17.42
46	0	--	2.10	16,448	74.0	32.0	19.159	18.998	16.89
47	0	--	2.10	16,907	74.0	31.9	19.159	18.758	16.68
48	0	--	2.10	16,807	74.2	31.8	19.159	18.637	16.58
49	2	A	4.19	1,993	78.3	161.3	18.834	66.853	65.51
50	2	A	4.19	2,107	78.2	162.1	18.834	66.372	64.95
51	2	A	4.19	2,128	78.2	162.0	18.834	66.613	65.17
52	2	A	4.19	2,109	78.2	162.5	18.834	66.853	65.41
53	2	A	4.32	2,167	77.9	98.1	18.904	43.386	42.37
54	2	A	4.32	2,176	77.7	98.4	18.904	43.888	42.97
55	2	A	4.32	2,121	77.8	98.5	18.904	43.647	42.75
56	2	A	4.32	2,113	77.8	98.4	18.904	43.286	42.40
57	2	A	4.24	2,189	77.3	56.6	18.983	25.611	25.07
58	2	A	4.24	2,155	77.4	56.5	18.983	25.972	25.43
59	2	A	4.24	2,155	77.5	56.5	18.983	25.852	25.31
60	2	A	4.24	2,190	77.5	56.5	18.983	25.611	25.07
61	2	A	4.25	2,181	77.2	31.9	18.983	13.707	13.40
62	2	A	4.25	2,173	77.3	32.0	18.983	13.948	13.64
63	2	A	4.25	2,161	77.3	32.0	18.983	13.948	13.65

TABLE I (continued)

A	B	C	D	E	F	G	H	I	J
Run No.	No. of Blades	Blade Type	Axial Flow lbs/min W	Fluid Viscosity Centipoises μ'	Fluid Temp.- °F	Rotor Speed rpm n'	Active Rotor Length Inches	Observed Torque Inch-lbs	Adjusted Torque Inch-lbs T'
64	2	A	4.25	2,157	77.3	32.0	18.983	13.707	13.41
65	2	A	4.29	1,974	78.6	31.8	18.983	15.751	15.47
66	2	A	4.29	2,047	78.3	31.9	18.983	15.511	15.22
67	2	A	4.29	2,091	78.4	31.8	18.983	15.632	15.34
68	2	A	4.29	2,112	78.3	31.8	18.983	15.511	15.22
69	2	A	9.52	2,139	78.4	31.8	19.075	15.511	15.20
70	2	A	9.52	2,112	78.3	31.7	19.075	15.632	15.33
71	2	A	9.52	2,117	78.2	31.9	19.075	15.511	15.21
72	2	A	9.52	2,115	78.3	31.8	19.075	15.511	15.21
73	2	A	9.58	2,149	78.1	57.8	19.075	28.136	27.58
74	2	A	9.58	2,143	78.1	58.0	19.075	27.535	26.98
75	2	A	9.58	2,118	78.3	58.0	19.075	27.776	27.25
76	2	A	9.58	2,118	78.2	58.1	19.075	27.535	26.99
77	2	A	4.36	2,160	77.9	58.1	18.971	27.415	26.86
78	2	A	4.36	2,149	78.2	58.1	18.971	27.776	27.23
79	2	A	4.36	2,128	78.1	58.1	18.971	27.535	27.00
80	2	A	4.36	2,117	78.3	58.1	18.871	27.295	26.75
81	2	A	4.33	2,118	78.5	97.3	18.942	44.730	43.83
82	2	A	4.33	2,112	78.3	97.5	18.942	44.730	43.84
83	2	A	4.33	2,068	78.5	97.6	18.942	44.128	43.26
84	2	A	4.33	2,077	78.4	97.6	18.942	43.046	42.17
85	2	A	9.75	2,127	78.2	97.8	19.008	43.166	42.25
86	2	A	9.75	2,072	78.4	97.9	19.008	43.046	42.12
87	2	A	9.75	2,075	78.3	97.9	19.008	42.565	41.65
88	2	A	9.75	2,041	78.6	98.1	19.008	42.084	41.19
89	2	A	9.97	2,101	79.2	159.6	18.922	67.454	65.99
90	2	A	9.97	2,077	79.0	161.0	18.922	67.214	65.75
91	2	A	9.97	2,039	79.1	161.5	18.922	66.973	65.53
92	2	A	9.97	2,018	79.2	161.9	18.922	66.613	65.19
93	2	A	4.64	2,035	80.1	160.9	18.871	65.636	64.26
94	2	A	4.64	2,008	80.2	162.0	18.871	64.070	62.68
95	2	A	4.64	2,007	80.4	162.5	18.871	64.341	62.96
96	2	A	4.64	1,995	80.6	162.4	18.871	64.672	63.29
97	2	A	2.89	8,398	75.4	31.6	19.123	48.577	47.38
98	2	A	2.89	8,643	75.0	31.6	19.123	48.577	47.35
99	2	A	2.89	8,478	75.1	31.6	19.123	48.577	47.37
100	2	A	2.89	8,030	75.3	31.6	19.123	48.336	47.21
101	2	A	4.36	8,178	75.5	31.6	19.160	48.697	47.52
102	2	A	4.36	8,323	75.6	31.6	19.160	47.374	46.17
103	2	A	4.36	8,160	75.9	31.5	19.160	47.855	46.68
104	2	A	4.36	8,183	75.6	31.6	19.160	47.855	46.69
105	2	A	4.46	8,178	75.9	57.0	19.145	83.567	81.45
106	2	A	4.46	8,118	76.0	57.1	19.145	82.004	79.89
107	2	A	4.46	8,023	76.2	57.0	19.145	81.403	79.32
108	2	A	4.46	7,905	76.2	57.1	19.145	83.207	81.15
109	2	A	2.93	7,870	76.6	57.1	19.068	82.004	79.97
110	2	A	2.93	8,125	77.0	57.1	19.068	80.922	78.85
111	2	A	2.93	8,010	77.3	57.1	19.068	80.207	78.14
112	2	A	2.93	7,865	77.1	57.1	19.068	81.283	79.27
113	2	A	2.99	7,528	77.6	94.0	19.010	122.164	119.01
114	2	A	2.99	7,533	77.8	94.3	19.010	120.240	117.08
115	2	A	2.99	7,513	78.1	94.6	19.010	119.769	116.60
116	2	A	2.99	7,560	79.0	94.3	19.010	122.164	119.01
117	2	A	4.77	7,545	78.2	94.5	19.069	121.563	118.38
118	2	A	4.77	7,745	78.4	94.6	19.069	120.020	116.73
119	2	A	4.77	7,548	78.5	94.9	19.069	119.639	116.44
120	2	A	4.77	7,495	78.8	95.0	19.069	118.436	115.24
121	2	A	4.95	7,135	80.7	145.5	19.026	164.729	160.08
122	2	A	4.95	7,275	81.0	145.1	19.026	161.482	156.83
123	2	A	4.95	7,183	81.1	145.7	19.026	160.039	155.34
124	2	A	4.95	7,003	81.5	145.9	19.026	160.280	155.68
125	2	A	3.35	6,653	81.8	146.5	18.961	156.192	151.94
126	2	A	3.35	6,940	83.5	146.5	18.961	155.711	151.29
127	2	A	3.35	6,790	81.1	147.1	18.961	153.907	149.49
128	2	A	3.35	6,345	83.9	147.6	18.961	152.104	148.00
129	2	A	2.87	12,053	74.6	31.4	19.161	76.462	74.76
130	2	A	2.87	12,920	74.4	31.4	19.161	75.150	73.32
131	2	A	2.87	13,067	74.3	31.2	19.161	75.150	73.33
132	2	A	2.87	12,620	74.4	31.1	19.161	73.346	71.58

TABLE I (continued)

A	B	C	D	E	F	C	H	I	J
Run No.	No. of Blades	Blade Type	Axial Flow lbs/min W	Fluid Viscosity Centipoises μ'	Fluid Temp.- °F	Rotor Speed rpm n'	Active Rotor Length Inches	Observed Torque Inch-lbs	Adjusted Torque Inch-lbs T'
133	2	A	2.70	13,073	74.5	55.6	19.115	122.284	119.01
134	2	A	2.70	13,497	74.7	55.6	19.115	123.848	120.45
135	2	A	2.70	13,257	75.0	55.6	19.115	124.569	121.24
136	2	A	2.70	13,177	75.2	55.6	19.115	125.170	121.87
137	2	A	2.65	12,160	75.6	90.2	19.063	186.612	181.67
138	2	A	2.65	12,500	76.8	90.6	19.063	187.334	182.23
139	2	A	2.65	12,247	77.1	90.9	19.063	184.328	179.33
140	2	A	2.65	12,180	77.0	90.7	19.063	186.011	181.11
141	2	A	3.66	11,287	76.3	31.2	19.210	75.751	74.14
142	2	A	3.66	12,267	76.1	31.1	19.210	73.347	71.59
143	2	A	3.66	11,917	76.0	31.2	19.210	72.385	70.68
144	2	A	3.66	12,233	76.3	31.1	19.210	72.866	71.11
145	2	A	3.78	12,490	76.8	55.5	19.170	128.898	125.75
146	2	A	3.78	12,910	76.6	55.6	19.170	129.860	126.56
147	2	A	3.78	12,387	77.2	55.6	19.170	123.487	120.34
148	2	A	3.78	12,120	77.1	55.6	19.170	125.651	122.58
149	2	A	3.88	11,923	78.1	89.0	19.138	181.924	177.12
150	2	A	3.88	12,097	78.5	89.5	19.138	175.070	170.15
151	2	A	3.88	12,140	78.4	90.0	19.138	177.835	172.89
152	2	A	3.88	11,553	78.8	90.5	19.138	171.102	166.35
153	2	A	1.58	17,877	78.6	31.0	19.156	114.348	111.80
154	2	A	1.58	19,443	78.4	31.0	19.156	113.627	110.88
155	2	A	1.58	19.477	78.5	31.0	19.156	113.627	110.88
156	2	A	1.58	19,610	78.4	31.0	19.156	115.791	113.04
157	2	A	1.59	19.533	79.2	59.4	19.112	190.460	185.31
158	2	A	1.59	19,247	80.0	59.5	19.112	187.694	182.54
159	2	A	1.59	18,890	80.4	59.8	19.112	186.251	181.15
160	2	A	1.59	19,370	80.4	59.5	19.112	190.700	185.50
161	2	A	1.59	18.400	80.6	86.4	19.076	257.313	250.16
162	2	A	1.68	17,810	32.5	87.8	19.076	253.947	246.92
163	2	A	1.68	17,650	83.6	87.8	19.076	252.744	245.79
164	2	A	1.68	17,890	82.5	87.8	19.076	254.428	247.38
165	2	A	2.46	19,853	79.8	31.0	19.187	113.627	110.83
166	2	A	2.46	19,477	79.7	31.1	19.187	111.823	109.07
167	2	A	2.46	19,183	80.0	31.0	19.187	111.823	109.12
168	2	A	2.46	19,273	79.9	31.0	19.187	111.463	108.71
169	2	A	2.51	19,107	80.3	54.2	19.158	182.404	177.75
170	2	A	2.51	19,387	80.2	54.2	19.158	181.322	176.62
171	2	A	2.51	19,040	80.3	54.3	19.158	179.638	174.99
172	2	A	2.51	18,947	80.3	54.2	19.158	179.879	175.33
173	2	A	2.53	17,840	81.5	84.5	19.115	257.193	250.39
174	2	A	2.53	18,607	81.3	86.2	19.115	256.712	249.41
175	2	A	2.53	18.007	81.5	87.1	19.115	252.624	245.57
176	2	A	2.53	17,330	83.8	86.9	19.115	250.340	243.54
177	1	A	1.61	19,710	77.3	31.0	18.933	79.979	77.33
178	1	A	1.61	20,650	77.3	31.0	18.933	79.979	77.18
179	1	A	1.61	20.925	77.5	31.0	18.933	78.896	76.05
180	1	A	1.61	20,500	77.5	31.0	18.933	77.813	75.04
181	1	A	1.64	20,650	77.8	54.6	18.456	134.447	130.15
182	1	A	1.64	20,725	77.7	54.5	18.456	135.409	131.16
183	1	A	1.64	20,825	77.8	54.2	18.456	135.289	131.04
184	1	A	1.64	20,650	77.9	54.2	18.456	135.890	131.69
185	1	A	1.62	20,900	77.7	83.0	17.67	210.439	206.44
186	1	A	1.62	20,900	77.8	83.0	17.67	207.794	203.79
187	1	A	1.62	20,900	77.8	82.9	17.67	213.926	209.93
188	1	A	1.62	20,775	77.8	82.7	17.67	214.046	210.15
189	0	--	2.48	14.123	79.7	32.0	19.150	16.472	14.63
190	0	--	2.48	14,423	79.8	32.0	19.150	16.593	14.74
191	0	--	2.48	13,920	80.0	32.0	19.150	16.472	14.63
192	0	--	2.48	13,777	80.0	32.0	19.150	16.472	14.63
193	0	--	2.36	13,930	80.2	56.1	19.111	29.819	26.58
194	0	--	2.36	13,933	80.0	56.7	19.111	29.819	26.58
195	0	--	2.36	14,107	79.9	56.5	19.111	30.180	26.85
196	0	--	2.36	13,847	79.8	56.6	19.111	29.940	26.65
197	0	--	2.21	14,727	78.5	97.1	19.043	53.266	47.45
198	0	--	2.21	14,683	78.8	97.1	19.043	52.885	47.10
199	0	--	2.21	14,180	78.9	97.5	19.043	52.304	46.60
200	0	--	2.21	14,153	78.9	97.6	19.043	52.304	46.60
201	0	--	2.28	14,047	80.6	158.3	18.900	80.921	72.43
202	0	--	2.28	12,963	81.5	159.5	18.900	79.698	71.40
203	0	--	2.28	12,893	82.4	160.1	18.900	78.997	70.70
204	0	--	2.28	12,880	82.4	160.5	18.900	78.637	70.45

TABLE I (continued)

A	B	C	D	E	F	G	H	I	J
Run No.	No. of Blades	Blade Type	Axial Flow lbs/min W	Fluid Viscosity Centipoises μ'	Fluid Temp.- °F	Rotor Speed rpm n'	Active Rotor Length Inches	Observed Torque Inch-lbs	Adjusted Torque Inch-lbs T'
205	0	--	1.57	16,287	80.5	152.5	18.930	105.691	94.40
206	0	--	1.57	16,160	81.3	154.7	18.930	107.133	95.80
207	0	--	1.57	16,080	82.1	155.3	18.930	108.817	97.10
208	0	--	1.57	15,827	83.0	156.4	18.930	108.937	97.25
209	0	--	1.57	15,373	83.7	159.9	18.930	107.133	95.80
210	0	--	1.55	16,820	80.9	97.4	19.038	63.968	57.00
211	0	--	1.55	16,867	80.9	97.2	19.069	66.372	59.05
212	0	--	1.55	16,880	81.0	97.4	19.069	65.771	58.55
213	0	--	1.55	16,897	81.3	97.6	19.045	64.449	57.40
214	0	--	1.64	16,847	80.9	58.0	19.120	39.800	35.42
215	0	--	1.64	16,783	80.9	58.0	19.120	39.439	35.12
216	0	--	1.64	16,810	81.0	58.0	19.120	39.559	35.20
217	0	--	1.64	16,610	81.3	58.0	19.120	39.199	34.88
218	0	--	1.73	16,863	80.9	32.0	19.191	21.884	19.47
219	0	--	1.73	17,287	80.8	32.0	19.168	22.124	19.67
220	0	--	1.73	16,903	80.9	31.9	19.208	23.086	20.53
221	0	--	1.73	16,953	81.0	32.0	19.208	22.605	20.07
222	0	--	1.66	16,127	82.0	145.3	18.919	103.045	92.15
223	0	--	1.66	15,850	84.0	155.2	18.919	102.564	91.65
224	0	--	1.66	15,610	84.7	156.3	18.919	102.204	91.50
225	0	--	1.66	15,107	85.4	157.2	18.919	101.242	90.55
226	0	--	3.86	5,140	83.1	160.5	18.960	36.673	32.75
227	0	--	3.86	5,095	82.9	162.4	18.915	39.198	35.07
228	0	--	3.86	5,080	83.2	163.2	18.915	41.362	36.95
229	0	--	3.86	5,110	83.3	163.5	18.915	42.685	38.20
230	0	--	3.86			163.6	18.915	43.647	
231	0	--	3.86			163.9	18.915	43.767	
232	0	--	3.72	5,335	82.6	161.4	18.860	36.673	32.85
233	0	--	3.72	5,255	82.8	162.7	18.860	34.629	31.05
234	0	--	3.72	5,210	82.7	163.4	18.860	33.426	29.95
235	0	--	3.72	5,180	82.9	164.4	18.860	33.186	29.75
236	0	--	3.91	5,200	82.3	98.7	19.000	24.890	22.22
237	0	--	3.91	5,235	82.8	98.9	19.000	27.295	24.35
238	0	--	3.91	5,250	83.0	98.7	19.000	27.655	24.68
239	0	--	3.91	5,190	82.8	98.7	19.000	28.257	25.21
240	0	--	3.91			98.5	19.000	28.978	
241	0	--	3.92	5,365	82.2	58.7	19.075	13.226	11.79
242	0	--	3.92	5,560	82.4	58.6	19.075	14.308	12.73
243	0	--	3.92	5,330	82.4	58.7	19.075	14.068	12.51
244	0	--	3.92	5,345	82.4	58.6	19.075	13.707	12.22
245	0	--	3.69	5,460	82.2	32.0	19.144	8.176	7.27
246	0	--	3.69	5,415	82.1	32.0	19.100	8.296	7.38
247	0	--	3.69	5,360	82.1	32.0	19.100	7.936	7.06
248	0	--	3.69	5,440	82.1	32.0	19.100	7.455	6.64
249	0	--	3.13	5,735	78.3	159.5	18.864	40.160	35.60
250	0	--	3.13	5,790	78.9	162.1	18.864	38.717	34.68
251	0	--	3.13	5,840	78.8	162.9	18.864	38.356	34.38
252	0	--	3.13	5,800	78.8	163.5	18.864	38.236	34.25
253	0	--	3.10	6,825	78.2	32.0	19.118	7.936	7.06
254	0	--	3.10	6,410	78.3	32.0	19.118	7.936	7.06
255	0	--	3.10	6,300	78.3	32.0	19.118	7.936	7.06
256	0	--	3.10	6,225	78.3	32.0	19.118	7.936	7.06
257	0	--	3.13	6,460	78.3	58.6	19.076	14.669	13.06
258	0	--	3.13	6,410	78.5	58.6	19.076	14.549	12.96
259	0	--	3.13	6,390	78.3	58.6	19.076	14.549	12.96
260	0	--	3.13	6,325	78.4	58.6	19.076	14.549	12.96
261	0	--	3.12	6,450	78.7	98.4	18.975	24.770	22.08
262	0	--	3.12	6,380	78.7	98.4	18.975	24.529	21.88
263	0	--	3.12	6,305	78.8	98.6	18.075	24.650	22.00
264	0	--	3.12	6,240	78.7	98.6	18.975	24.409	21.79
265	1	A	2.49	8,510	75.6	137.5	18.332	134.909	130.66
266	1	A	2.49	8,750	75.7	136.5	18.332	132.024	127.67
267	1	A	2.49	8,670	75.7	137.0	18.332	132.144	127.89
268	1	A	2.49	8,690	75.7	135.0	18.332	132.384	128.18
269	1	A	2.49	8.655	74.9	91.5	18.489	103.407	100.39
270	1	A	2.49	8,720	74.8	91.1	18.489	99.920	96.92
271	1	A	2.49	8,690	75.0	91.1	18.489	103.152	100.12
272	1	A	2.49	8,670	75.1	91.1	18.489	103.286	100.29
273	1	A	2.47	9,190	74.5	56.2	18.542	63.968	61.99
274	1	A	2.47	9,100	74.6	56.3	18.542	63.126	61.13
275	1	A	2.47	8,730	74.7	56.2	18.542	63.246	61.35
276	1	A	2.47	8,870	74.8	56.2	18.542	63.246	61.27

TABLE I (continued)

A	B	C	D	E	F	G	H	I	J
Run No.	No. of Blades	Blade Type	Axial Flow lbs/min W	Fluid Viscosity Centipoises μ'	Fluid Temp. ^{o}F	Rotor Speed rpm n'	Active Rotor Length Inches	Observed Torque Inch-lbs	Adjusted Torque Inch-lbs T'
277	1	A	2.40	7,710	75.1	31.4	18.690	29.819	28.84
278	1	A	2.40	8,450	74.8	31.4	18.690	32.623	31.53
279	1	A	2.40	8,610	74.7	31.3	18.690	33.066	31.97
280	1	A	2.40	8,895	74.7	31.3	18.690	32.942	31.81
281	1	A	2.80	3,391	74.7	31.6	18.674	15.873	15.43
282	1	A	2.80	3,408	74.0	31.6	18.674	14.309	13.87
283	1	A	2.80	3,115	73.8	31.7	18.674	12.386	11.99
284	1	A	2.80	3,153	73.8	31.6	18.674	11.303	10.89
285	1	A	2.64	3,385	73.8	57.1	18.541	29.099	28.35
286	1	A	2.64	3,378	73.6	57.1	18.541	30.783	30.03
287	1	A	2.64	3,481	73.7	57.1	18.541	30.788	30.01
288	1	A	2.64	3,465	73.7	57.1	18.541	31.023	30.26
289	1	A	2.61	3,531	73.8	95.0	18.557	43.899	42.60
290	1	A	2.61	3,487	73.8	94.5	18.557	44.981	43.71
291	1	A	2.61	3,483	74.0	94.4	18.557	44.500	43.21
292	1	A	2.61	3,522	73.9	94.6	18.557	45.702	44.41
293	1	A	2.62	3,622	73.9	151.2	18.418	66.744	64.69
294	1	A	2.62	3,531	74.0	152.4	18.418	63.017	61.02
295	1	A	2.62	3,559	74.0	150.9	18.418	63.378	61.39
296	1	A	2.62	3,541	74.1	152.9	18.418	64.460	62.44
297	1	A	2.63	14,417	75.1	87.5	18.779	148.016	142.72
298	1	A	2.63	15,100	74.8	87.1	18.779	148.497	143.05
299	1	A	2.63	14,907	75.1	86.9	18.779	149.338	144.04
300	1	A	2.63	14,860	75.1	86.3	18.779	152.585	147.39
301	1	A	2.60	14,087	74.7	55.3	18.850	97.996	94.75
302	1	A	2.60	14,353	74.8	55.2	18.850	94.870	91.54
303	1	A	2.60	14,527	74.8	55.3	18.850	98.357	94.99
304	1	A	2.60	14,427	75.0	55.3	18.850	98.357	95.01
305	1	A	2.57	11,977	75.2	31.1	18.850	54.108	52.54
306	1	A	2.57	13,537	74.8	31.1	18.850	55.550	53.77
307	1	A	2.57	13,683	74.8	31.1	18.850	55.310	53.51
308	1	A	2.57	14,227	74.6	31.1	18.850	55.550	53.67
309	2	B	2.39	11,957	77.3	91.6	19.077	104.369	99.42
310	2	B	2.39	13,120	77.1	91.5	19.077	105.451	100.15
311	2	B	2.39	13,640	77.1	92.6	19.077	105.451	99.65
312	2	B	2.40	13,147	77.9	142.8	19.014	149.218	140.82
313	2	B	2.40	12,890	78.3	144.1	19.014	142.124	133.87
314	2	B	2.40	12,697	80.6	144.6	19.014	139.839	131.64
315	2	B	2.34	14,733	77.5	57.0	19.129	65.290	61.49
316	2	B	2.34	14,823	76.3	57.1	19.129	63.126	59.31
317	2	B	2.34	14,473	76.8	57.0	19.129	62.284	58.56
318	2	B	2.59	14,580	76.5	31.6	19.190	34.750	32.64
319	2	B	2.59	14,593	76.6	31.5	19.190	34.630	32.53
320	2	B	2.59	14,400	76.1	31.5	19.190	35.712	33.66
321	2	B	2.59	15,017	76.3	31.5	19.190	36.073	33.90
322	2	B	1.90	4,545	75.5	151.6	18.866	69.979	67.08
323	2	B	1.90	4,915	76.1	155.1	18.866	69.979	66.78
324	2	B	1.90	4,790	76.6	156.1	18.866	69.258	66.14
325	2	B	2.08	5,165	76.4	96.3	18.947	43.166	41.00
326	2	B	2.08	4,930	75.8	96.4	18.947	42.084	40.02
327	2	B	2.08	4,965	75.6	96.4	18.047	41.483	39.38
328	2	B	2.14	5,000	75.2	57.8	19.006	25,371	24.10
329	2	B	2.14	4,990	75.0	57.9	19.006	24.890	23.61
330	2	B	2.14	5,000	74.9	57.9	19.006	24.409	23.15
331	2	B	2.06	5,050	74.8	31.6	19.033	13.587	12.88
332	2	B	2.06	5,230	74.5	31.6	19.033	13.828	13.10
333	2	B	2.06	5,130	74.3	31.6	19.033	13.707	12.99
334	2	B	3.74	9,570	76.2	31.3	19.207	27.896	26.52
335	2	B	3.74	10,017	76.0	31.5	19.207	28.016	26.55
336	2	B	3.74	9,703	76.2	31.5	19.207	27.535	26.13
337	2	B	3.83	9,635	76.6	56.9	19.139	49.419	46.92
338	2	B	3.83	9,643	76.5	56.9	19.139	48.457	45.96
339	2	B	3.83	9,735	76.8	57.0	19.139	48.697	46.15
340	2	B	3.92	9,298	77.4	94.2	19.069	75.391	71.49
341	2	B	3.92	9,470	78.0	94.4	19.069	75.872	71.87
342	2	B	3.92	8,143	78.2	94.5	19.069	74.308	70.46
343	2	B	4.05	8,763	79.3	151.2	18.968	109.178	103.33
344	2	B	4.05	8,728	80.1	152.5	18.968	105.691	99.74
345	2	B	4.05	8,570	80.5	152.7	18.968	105.451	99.70
346	2	B	2.54	18,587	77.5	31.0	19.236	50.501	47.48
347	2	B	2.54	19,033	78.0	31.2	19.236	49.779	47.04
348	2	B	2.54	18,517	77.8	31.2	19.236	49.418	46.76

TABLE I (continued)

A	B	C	D	E	F	G	H	I	J
Run No.	No. of Blades	Blade Type	Axial Flow lbs/min W	Fluid Viscosity Centipoises μ'	Fluid Temp.- °F	Rotor Speed rpm n'	Active Rotor Length Inches	Observed Torque Inch-lbs	Adjusted Torque Inch-lbs T'
349	2	B	2.58	19,040	78.0	55.6	19.163	91.262	86.46
350	2	B	2.58	19,777	78.0	55.6	19.163	91.142	86.09
351	2	B	2.58	18,660	79.1	55.7	19.163	88.737	84.04
352	2	B	2.64	18,267	79.2	88.7	19.100	141.643	134.24
353	2	B	2.64	19,140	79.0	88.4	19.100	141.763	134.11
354	2	B	2.64	18,723	78.5	88.0	19.100	143.326	135.88
355	4	A	2.35	17,987	77.8	30.6	19.237	133.827	131.26
356	4	A	2.35	19,720	77.7	30.5	19.237	134.308	131.52
357	4	A	2.35	19,723	77.4	30.6	19.237	131.903	129.11
358	4	A	2.39	19,260	78.9	54.5	19.169	217.394	212.64
359	4	A	2.39	20,250	78.5	54.4	19.160	217.875	212.83
360	4	A	2.39	19,890	78.5	54.4	19.169	216.312	211.36
361	4	A	2.46	18,960	78.9	84.0	19.100	286.172	278.92
362	4	A	2.46	19,173	78.9	84.7	19.100	287.614	280.31
363	4	A	2.46	19,100	79.4	85.6	19.100	285.811	278.41
364	4	A	4.55	5,220	75.6	31.1	19.108	45.802	45.08
365	4	A	4.55	4,925	75.1	31.1	19.108	41.363	40.67
366	4	A	4.55	4,860	75.6	81.2	19.108	40.641	39.96
367	4	A	4.44	5,000	75.7	56.9	19.064	70.340	69.04
368	4	A	4.44	4,940	75.9	56.9	19.064	69.859	68.62
369	4	A	4.44	4,890	75.8	56.9	19.064	70.821	69.58
370	4	A	4.40	4,870	76.2	91.3	19.032	111.102	109.12
371	4	A	4.40	4,840	76.5	94.1	19.032	109.900	107.85
372	4	A	4.40	4,900	76.2	93.9	10.032	111.342	109.28
373	4	A	3.62	8,360	72.4	31.1	19.200	73.467	72.27
374	4	A	3.62	8,680	72.4	31.1	19.200	73.467	72.23
375	4	A	3.62	8,915	72.2	31.0	19.200	75.270	73.99
376	4	A	3.76	9,170	73.0	55.9	19.143	125.531	123.20
377	4	A	3.76	9,070	72.8	56.0	19.143	123.247	120.97
378	4	A	3.76	9,070	72.5	56.0	19.143	122.645	120.36
379	4	A	3.81	8,790	73.5	90.4	19.100	188.295	184.70
380	4	A	3.81	8,810	73.3	90.6	19.100	186.612	183.01
381	4	A	3.81	8,795	73.4	90.6	19.100	187.454	183.85
382	4	A	2.96	16,073	72.7	30.6	19.216	114.108	111.85
383	4	A	2.96	16,633	73.1	30.6	19.216	111.823	109.49
384	4	A	2.96	16,700	72.9	30.7	19.216	112.304	109.93
385	4	A	3.15	15,443	74.3	54.9	19.175	188.416	184.54
386	4	A	3.15	16,030	74.2	55.0	19.175	183.847	179.85
387	4	A	3.15	15,787	74.1	55.0	19.175	183.606	179.66
388	4	A	3.33	14,220	76.1	86.1	19.125	268.856	263.31
389	4	A	3.33	15,333	75.8	86.3	19.125	266.452	260.45
390	4	A	3.33	14,633	76.0	86.5	19.125	266.692	260.99

TABLE II

MECHANICAL EFFECTS DATA - 2 AND 4 TYPE A BLADES

A	B	C	D	E	F	G	H	I	J
Line No.	Data Sheet No.	No. of Type A Blades	Solution % Ucon	Axial Flow Rate - W lbs/hr.	Fluid Viscosity Centipoises μ'	Rotor Speed rpm n'	Fluid Temp. Rise t - °F	$\frac{\mu'}{n}$	$\frac{W\ Cp\ \Delta t}{n'3}$
1	1T	4	83.0	137	12,910	30.8	1.6	419	0.00443
2	6T	4	83.0	197	13,372	30.9	1.0	432	0.00394
3	7T	4	83.0	208	14,374	55.6	2.7	258	0.00193
4	8T	4	83.0	210	12,792	89.6	6.1	143	0.00105
5	15T	4	83.0	192	13,580	30.7	1.1	442	0.00430
6	18T	4	77.5	222	11,500	31.0	0.7	371	0.00323
7	19T	4	77.5	232	10,900	56.1	2.0	194	0.00163
8	20T	4	77.5	237	10,100	91.8	4.2	110	0.00080
9	29T	2	77.5	237	9,400	31.2	0.6	301	0.00290
10	30T	2	77.5	246	9,049	56.9	1.3	159	0.00108
11	31T	2	77.5	253	8,652	94.2	2.0	92	9.00054
12	40T	2	83.0	212	12,319	31.0	0.9	398	0.00378
13	41T	2	83.0	225	12,414	51.3	2.1	242	0.00206
14	42T	2	83.0	237	11,755	91.9	4.5	128	0.00081

TABLE III

MECHANICAL EFFECTS DATA - SMOOTH ROTOR

A	B	C	D	E	F	G	H	I	J
Line No.	Data Sheet No.	No. of Blades	Solution % Ucon	Axial Flow Rate - W lbs/hr	Fluid Viscosity Centipoises μ'	Rotor Speed rpm n'	Fluid Temp. Rise t - ^oF	$\frac{\mu'}{n'}$	$\frac{W\ Cp\ \Delta t}{n'^3}$
1	56T	0	83%	193	16,100	31.4	0.3	513	0.00110
2	57T	0	83%	199	15,534	57.5	0.8	270	0.00049
3	58%	0	83%	204	14,829	96.4	1.9	154	0.00026
4	59T	0	83%	212	13,759	158.6	4.2	87	0.0013

TABLE IV

HEAT TRANSFER DATA - 2 AND 4 TYPE A BLADES

A	B	C	D	E	F	G	H	I	J	K	L
Line No.	Data Sheet No.	Observed Viscosity Centipoises μ'	Rotor Speed rpm n'	Axial Flow Rate lbs/hr W	Solution % Ucon	Temp. Rise Mech ^oR $\Delta t_{mech.}$	Net Temp Rise ^oF Δt_{net}	LMTD Wall to Fluid ^oF	Heat Transfer Coeff h Btu/hr;ft^2;^oF	$\frac{C_p \rho\ sd^2}{k}$	$\frac{hd}{k}$ (avg. h)
					4 Blades on Rotor - Heating Fluid						
1	2T	13,659	30.9	148	83 %	1.5	1.8	4.6	39.8	3,520	13.6
2							2.1	5.3	40.3		
3							2.0	4.5	45.2		
4							2.2	5.4	41.4		
5	9T	12,215	56.3	234	83 %	2.3	2.5	4.5	89.4	6,410	24.2
6							2.3	5.8	63.8		
7							2.1	4.9	69.0		
8	11T	10,367	89.4	207	83 %	4.6	6.6	12.0	78.2	10,180	26.3
9							6.8	12.3	78.6		
10							6.9	11.6	84.7		
11	16T	13,107	31.0	207	83 %	1.0	4.8	14.6	46.8	3,530	15.8
12							5.0	14.4	49.4		
13							5.0	14.1	50.4		
14	21T	8,455	31.1	253	77.5%	0.4	3.5	13.5	47.4	3,440	15.3
15							3.7	12.9	52.4		
16							3.8	13.1	53.0		
17	25T	9,035	56.3	219	77.5%	3.1	6.3	12.0	83.0	6,230	23.7
18							6.3	12.3	81.0		
19							5.8	12.7	72.2		
20	27T	8,078	92.9	225	77.5%	3.1	7.3	9.7	130.8	10,250	37.6
21							6.9	9.2	121.9		
22							6.7	9.7	121.0		
					4 Blades on Rotor - Cooling Fluid						
23	4T	18,817	30.6	149	83.0%	2.2	-12.2	21.3	58.6	3,480	20.5
24							-12.9	20.6	64.1		
25							-13.1	20.6	65.7		
26	14T	16,839	86.7	211	83.0%	8.0	-13.1	16.9	112.3	9,860	38.2
27							-13.7	16.3	122.0		
28							-13.7	17.0	117.0		
29	23T	12,215	30.9	229	77.5%	0.8	-7.8	21.4	60.3	3,420	17.6
30							-7.8	21.7	59.4		
31							-7.6	22.2	56.6		
32	26T	12,907	55.8	237	77.5%	2.2	-10.2	21.5	81.2	6,170	26.1
33							-10.7	20.8	88.1		
							-10.9	20.7	90.2		
35	28T	12,352	90.6	248	77.5%	4.6	-11.8	19.4	109.0	10,020	33.0
36							-11.9	19.7	108.2		
37							-12.1	19.6	110.7		

TABLE IV (continued)

A	B	C	D	E	F	G	H	I	J	K	L
Line No.	Data Sheet No.	Observed Viscosity Centipoises μ'	Rotor Speed rpm n'	Axial Flow Rate lbs/hr W	Solution % Ucon	Temp. Rise Mech. ^{o}F $\Delta t_{mech.}$	Net Temp. Rise ^{o}F Δt_{net}	LMTD Wall to Fluid ^{o}F	Heat Transfer Coeff. h Btu/hr;ft^2;^{o}F	$\frac{C_p \rho sd^2}{k}$	$\frac{hd}{k}$ (avg. h)
					2 Blades on Rotor - Heating Fluid						
38	32T	8,527	31.3	263	77.5%	0.4	2.1	10.9	36.6	1,740	12.3
39							2.3	10.2	42.9		
							2.5	11.1	42.8		
41	36T	9,254	57.0	235	77.5%	1.5	2.4	14.0	29.1	3,140	9.3
42							2.6	13.2	33.4		
43							2.5	14.1	30.1		
44	43T	11,288	31.2	256	83.0%	0.7	2.7	11.8	40.3	1,770	13.0
45							2.7	11.4	41.7		
46							2.5	11.8	37.3		
47	47T	11,659	56.7	228	83.0%	2.2	3.1	14.5	33.5	3,230	9.1
48							2.6	15.6	26.1		
49							2.4	15.9	23.7		
50	53T	12,492	56.7	224	83.0%	2.5	5.5	13.2	64.2	3,230	19.9
51							5.4	14.0	59.4		
52							5.3	13.9	58.7		
53	55T	11,775	93.0	229	83.0%	5.2	3.9	12.9	47.6	5,290	16.4
54							4.3	12.7	53.3		
55							4.0	12.6	50.0		
					2 Blades on Rotor - Cooling Fluid						
56	34T	10,822	31.1	256	77.5%	0.6	-5.7	30.4	34.7	1,720	11.1
57							-6.1	29.5	38.2		
58							-6.0	29.5	37.6		
59	37T	11,097	56.6	242	77.5%	1.9	-5.5	23.6	40.7	3,130	13.0
60							-5.9	23.3	44.3		
61							-5.9	23.2	44.5		
62	39T	10,584	92.8	249	77.5%	3.9	-6.0	21.7	49.7	5,120	16.0
63							-6.5	21.5	54.4		
64							-6.4	21.4	53.8		
65	45T	14,157	31.1	255	83.0%	0.9	-5.4	30.4	31.1	1,770	11.4
66							-6.2	29.7	36.6		
67							-6.4	30.1	37.3		
68	48T	14,123	55.9	246	83.0%	2.6	-6.6	28.7	38.9	3,180	13.4
69							-6.9	28.3	41.2		
70							-7.1	28.2	42.6		
71	50T	13,454	89.8	253	83.0%	5.2	-8.1	30.9	45.6	5,110	15.1
72							-8.3	31.1	46.4		
73							-8.3	31.0	46.6		

TABLE V

HEAT TRANSFER DATA - SMOOTH ROTOR

A	B	C	D	E	F	G	H	I	J	K	L
Line No.	Data Sheet No.	Observed Viscosity Centipoises μ'	Rotor Speed rpm n'	Axial Flow Rate lbs/hr W	Solution % Ucon	Temp. Rise Mech. ^oF $\Delta t_{mech.}$	Net Temp Rise ^oF Δt_{net}	LMTD Wall to Fluid ^oF	Heat Transfer Coeff. Btu/hr;ft^2;^oF h	$\frac{C_p \rho n d^2}{k}$	$\frac{hd}{k}$ (Avg. h)
						Heating Fluid					
1	62T	13,210	57.8	218	83.0%	0.6	0.7	19.1	57.1	1,650	13.5
2							0.7	20.2	54.0		
3	70T						0.7	19.6	55.7		
4							0.3	19.4	22.4		
5							0.3	20.2	21.5		
6							0.5	19.0	38.2		
7	64T	12,989	97.1	223	83.0%	1.5	0.5	19.8	38.7	2,770	13.4
8							0.5	19.9	38.5		
9							0.6	20.0	46.0		
10	66T	12,150	160.4	224	83.0%	3.4	0.4	17.1	36.0	4,560	11.7
11							0.3	17.7	27.0		
12							0.5	17.3	45.0		
13	68T	12,139	31.3	208	83.0%	0.2	0.7	19.9	50.3	892	14.7
14							0.5	20.0	35.9		
15							0.7	20.5	48.8		
						Cooling Fluid					
16	63T	14,419	57.9	228	83.0%	0.6	-0.5	26.0	30.2	1,640	12.5
17							-0.6	25.9	36.3		
18							-0.8	25.8	48.7		
19	65T	13,749	97.1	223	83.0%	1.5	-0.6	27.0	34.7	2,770	12.6
20							-0.7	26.9	40.6		
21							-0.7	26.9	40.6		
22	67T	12,948	159.9	246	83.0%	3.4	-0.5	29.1	29.1	4,550	14.4
23							-0.9	29.4	51.7		
24							-0.9	29.6	51.4		
25	69T	14,530	31.3	214	83.0%	0.2	-0.1	24.6	6.0	892	9.7
26							-0.5	24.8	29.7		
27							-0.5	24.7	29.8		

BIBLIOGRAPHY

1. Bjorklund, I. S., and Kays, W. M. "Heat Transfer Between Concentric Rotating Cylinders." ASME Paper No. 58-A-99, 1958.

2. Curme and Johnston. "Glycols" ACS Monograph No. 114, Reinhold Publishling Corp., (1952) 280-282.

3. Gazley, Carl Jr. "Heat Transfer Characteristics of the Rotational and Axial Flow Between Concentric Cylinders." Trans. ASME, 80, No. 1, (1958) 79-90.

4. Goldstein, S. "The Stability of Viscous Fluid Flow Between Rotating Cylinders." Proceedings of the Cambridge Philosophical Society, 33, (1937) 41-61.

5. Green, Henry. Industrial Rheology and Rheological Structures. John Wiley, New York, 1949.

6. Houlton, H. G. "Heat Transfer in the Votator." Ind. and Eng. Chem., 36, No. 6, (1944) 522-528.

7. Jacob, M. and Rees, K. A. Trans. AIChE, 37, (1941) 619 - ... .

8. Kaye, Joseph and Elgar, E. C. "Modes of Adiabatic and Diabatic Fluid Flow in an Annulus with an Inner Rotating Cylinder." Trans. ASME, 80, (1958) 753-765.

9. Kern, D. Q. "Speculative Process Design." Chemical Engineering, (October 5, 1959) 127-142.

10. Kool, J. "Heat Transfer in Scraped Vessels and Pipes Handling Viscous Materials." Trans. Instn. Chem. Engrs., 36, (1958) 253-258.

11. Perry, E. and Reese, F. E. "Heat Transfer Processing Viscous Materials." Chemical Engineering Progress, 47, No. 7, (1951) 354-362.

12. Skelland, A.H.P. Chemical Eng. Science, 7, (1941) 166 - ... .

13. Skelland, A.H.P. and Leung, L. S. Power Consumption in a Scraped-Surface Heat Exchanger. AICHE-ASME Fourth National Heat Transfer Conference, Preprint 33, 1960.

14. Skelland, A.H.P., Oliver, D. R., and Tooke, S. Heat Transfer in a Water-Cooled Scraped-Surface Heat Exchanger. AIChE-ASME Fourth National Heat Transfer Conference, Preprint 33, 1960.

15. Taylor, G. I. "Stability of a Viscous Liquid Contained Between Two Rotating Cylinders." Philosophical Transactions of the Royal Society of London, Series A, 223, (1923) 289-343.

16. Westervelt, F. H. A Study of Automatic System Simulation Programming and the Analysis of the Behavior of Physical Systems Using an Internally Stored Program Computer. PhD. Thesis at The University of Michigan, Ann Arbor, Michigan, October 1960.